CARBON FIBER REINFORCED LITHIUM-ION BATTERY COMPOSITES WITH HIGHER MECHANICAL STRENGTH: MULTIFUNCTIONAL POWER INTEGRATION FOR STRUCTURAL APPLICATIONS

by

Mayur Shrikant Jadhav

A Thesis

Submitted to the Faculty of Purdue University

In Partial Fulfillment of the Requirements for the degree of

Master of Science in Mechanical Engineering

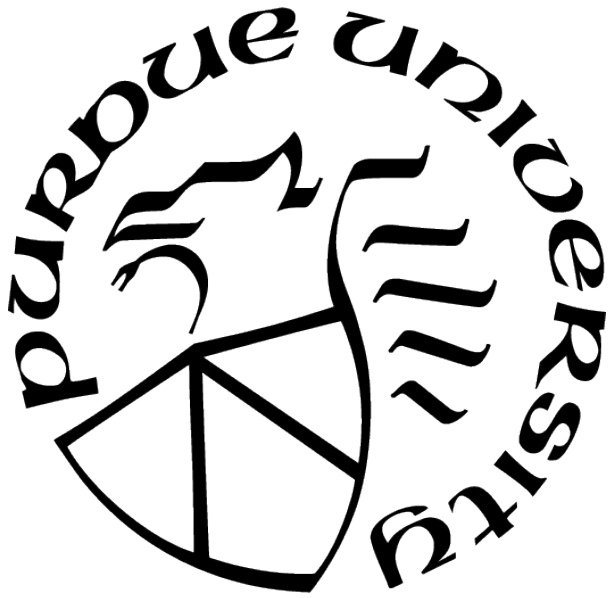

Department of Mechanical and Energy Engineering

Indianapolis, Indiana

August 2021

THE PURDUE UNIVERSITY GRADUATE SCHOOL
STATEMENT OF COMMITTEE APPROVAL

Dr. Mangilal Agarwal, Co-Chair

Department of Mechanical and Energy Engineering

Dr. Hamid Dalir, Co-Chair

Department of Mechanical and Energy Engineering

Dr. Jing Zhang

Department of Mechanical and Energy Engineering

Approved by:

Dr. Jie Chen

Dedicated to my Mother and Father

ACKNOWLEDGMENTS

First, I thank my professors for their supervision and support, initiating this project and providing comments and suggestions all the way until now. The study described in this thesis has been conducted at the Integrated Nanotechnology Development Institute (INDI) of Indiana University-Purdue University Indianapolis (IUPUI), under the guidance of Dr. Mangilal Agarwal and Dr. Hamid Dalir.

I would especially thank my project mentor Pias Biswas for helping me with the sample preparation of electrospinning of nanocomposite scaffolds and understand the fundamentals of energy storage devices right from the fabrication of lithium-ion batteries towards testing it. I would also thank to Asel Ananda for providing technical assistance in the experimentation process and Dr. Amanda Siegel for her supervision on planning and overseeing test plans and technical support. Without their help, I would never have been able to accomplish my research.

Also, I would like to thank Mr. Kevin Carr and Dr. Daniel Minner for their great efforts and support during my experimental tests and characterization at INDI. My sincere appreciation towards Ashwin Gaonkar for helping me with formatting of the draft, Kayla Maxey from Department of Biomedical Engineering (IUPUI) for helping me use their test equipment in my experimentation process and Yikang Yu from Electronic and Electrochemical Material and Devices Laboratory (IUPUI) for using their equipment in battery testing. I am thankful to all my amazing friends, lab mates, and roommates for their support, and the happiest memories in all these times and for making my time at IUPUI unforgettable for the rest of my life.

My deepest gratitude goes towards my lovely family, my parents and my sister for their support, unconditional love and encouragement. Finally, my special thanks to Vidya for being there for me this entire time motivating me to pursue my ambitions and continue to be a crucial part of my life.

TABLE OF CONTENTS

LIST OF TABLES 7

LIST OF FIGURES 8

ABBREVIATIONS 10

ABSTRACT 12

1 INTRODUCTION 13

1.1 Problem Statement 13

1.2 Literature Review 14

1.2.1 Composite Materials: Overview 14

1.2.2 Classification of Composite Materials 16

1.2.3 Properties of Composite Materials 19

1.2.4 Ply-Orientation of Different Laminate Types 20

1.2.5 Carbon Nano Tubes 23

1.2.6 Impact Damage Resistance of CNT-FRP Composites 24

1.2.7 Electrospinning of CNT Composite Fibres 25

1.2.8 Energy Storage Systems 27

1.2.9 Damage Evolution in Pouch Cell Subjected to Indentation Loads . . 31

1.2.10 Multifunction Energy Storage Systems 33

1.2.11 Testing and Performance of Multi-functional Composite Structures . 37

2 EXPERIMENTAL PROCEDURES 43

2.1 Air-spraying and Electrospinning Solution Preparation 43

2.1.1 Electrospun CFRP Facesheets Sample Preparation 44

2.1.2 CFRP Facesheets Sample Preparation 44

2.1.3 Air Sprayed CFRP Facesheets Sample Preparation 46

2.1.4 Assembly of the Batteries Inside the CFRP Samples 46

2.2 Mechanical Properties 49

2.2.1 Quasi-Static Three-Point Bending 49
2.2.2 Tensile Testing 50
2.2.3 Barely Visible Impact Damage (BVID) 52
2.2.4 Electrical Conductivity 52
2.2.5 Electrochemical Characterization 53

3 RESULTS AND DISCUSSION 55
3.1 Mechanical Properties 55
3.1.1 Quasi-Static Three-Point Bending Test 55
3.1.2 Flexural Rigidity 58
3.1.3 BVID Testing 61
3.1.4 Electrochemical Characterization Results 61

4 CONCLUSION 66

5 OPPORTUNITIES AND FUTURE RESEARCH 67

REFERENCES 68

LIST OF TABLES

3.1 Comparison between Electrospun and Electrospun Thermoplastic 57

LIST OF FIGURES

1.1 Composite Constituent Materials And Manufacturing Selections [7] 16

1.2 Fiber Reinforced Polymers (FRPs) 17

1.3 Ceramic Matrix Composites (CMCs) Diagram 17

1.4 Metal Matrix Composites (MMCs) 18

1.5 Sandwich Structure Composites (SSCs) 18

1.6 Laminates 19

1.7 SEM Of A Multiscale CNT-CFRP Composite [10] 23

1.8 SEM Images Of Carbon Fibers (A) Before And (B) After CNT Growth [10] . . 24

1.9 Time Vs Applied Load During Impact Test Of Multiscale CFRP Composites With 0, 5, 10 wt.% Cup-Stacked CNTs In Epoxy Matrix [11] 25

1.10 Electrospinning Methods [13] 27

1.11 Plot of Energy Storage Ragone [15] 28

1.12 Categorization Of Energy Storage Systems [16] 30

1.13 Setup of Loading And Measurement Pouch Cell Indentation: (Top) Setup of Test, And (Bottom) Composition, Thickness Distribution Of Pouch Cell And The Voltage Measurement Outline Of Fracture Sequence Analysis [19] 33

1.14 Carbon FRP laminate with an embedded LiPo battery Representation [27] . . . 35

1.15 Energy Storage Composites Laminates with an Embedded TFB [29] 36

1.16 (a)Schematic of Li-Ion Bicells; (b)Li-Ion Bicells within a Carbon Weave Pouch . 37

1.17 Vertical Bicells And Aluminum Triangular Corrugation Used In The Core Of A Sandwich Composite 37

1.18 Sample Surface Representing The Areas Of (Top) Global, (Middle) Local And (Bottom) Far-Field Strain As Measured With DIC. Dashed Lines Show An Embedded Battery Location [30] 38

1.19 Schematic Of Experimental Tension Test [30] 39

1.20 The Compression Test Conducted On The LiPo Battery [27] 40

1.21 Cross-Section Views Of The Composite Laminate Displaying Vertically Arranged Two Embedded Batteries (X-Ray CT Image) [27] 41

1.22 Laser Doppler Vibrometry Experiment Setup [33] 42

2.1 Electrospinning Schematic 45

2.2 CFRP Structure Preparation 45
2.3 Air-Spray Sample Preparation 46
2.4 Schematic Of CFRP Structure Assembly 47
2.5 Assembly Of CFRP Structure 48
2.6 Tensile Testing Sample Preparation 49
2.7 Schematic Of Quasistatic Three-Point Bending Testing 50
2.8 Tensile Test Setup 51
2.9 Load Vs Displacement Characteristics For Air-Sprayed And CFRP Samples . . 51
2.10 Electrical Conductivity Test setup 53
2.11 MESC Cyclic Testing Setup 54
3.1 Load V Displacement Curves for Asymmetric Orientation Samples 56
3.2 Load V Displacement for Symmetric Orientation Samples 56
3.3 Load V Displacement Curves for Comparison between Electrospun CFRP Cell and Electrospun Thermoplastic CFRP Cell 57
3.4 Load V Displacement Curves for CFRP Structure Without Batteries 58
3.5 Stress V Strain for Asymmetric Orientation Samples 59
3.6 Stress V Strain for Symmetric Orientation Samples 59
3.7 Stress V Strain for electrospun and electrospun with thermoplastic sheet insert 60
3.8 Stress V Strain for electrospun and CFRP samples without batteries. 60
3.9 CFRP Cell V Electrospun Cell on 16.50 J Impact 61
3.10 Capacity Vs Cycles for MESC Cells 62
3.11 Voltage Vs Capacity for 1st Cycle MESC Cells 63
3.12 Voltage Vs Capacity for 2nd Cycle MESC Cell 63
3.13 Voltage Vs Capacity for 3rd Cycle MESC Cell 64
3.14 Voltage Vs Capacity for 31st Cycle MESC Cell 64
3.15 Voltage Vs Capacity for 32nd MESC Cell 65
3.16 Voltage Vs Capacity for 33rd MESC Cell 65

ABBREVIATIONS

μm	Micrometer
2D	Two-Dimensional
3D	Three-Dimensional
ASTM	American Society For Testing And Materials
BVID	Barely Visible Impact Damage
cm	Centi-Meter
CCD	Charged-Coupled Devices
CFRP	Carbon Fiber-Reinforced Polymer
CMC	Ceramic Matrix Composites
CNT	Carbon Nanotubes
DIC	Digital Image Correlation
DMF	Dimethylformamide
EES	Electrical Energy Storage
EMI	Electromagnetic Interference Shielding
FRP	Fiber Reinforced Polymer
FE	Finite Element
GFRP	Glass Fibers Fortified Polymer
GHz	Giga Hertz
GPa	Giga-Pascal
GRP	Glass Reinforced Polymer
Hz	Hertz
kV	Kilovolt
Li-Po	Lithium Polymer Battery
LDV	Laser Scanning Doppler Vibrometry
MB	Masterbatch
MHz	Mega Hertz
ml	Milliliters
mm	Millimeters

MMC	Metal Matrix Composites
MESC	Multifunctional Energy Storage Composites
mW	Milliwatt
MWCNT	Multiwalled Carbon Nanotubes
Nm	Nanometer
RVE	Representative Volume Element
SSC	Sandwich Structure Composites
SEM	Scanning Electron Microscopy
SDC	Structural Dielectric Capacitor
SWCNT	Single Walled Carbon Nanotubes
TFB	Thin Film Batteries
VARTM	Vacuum Assisted Resin Transfer Molding Process

ABSTRACT

This study proposes and evaluates a multi-functional carbon fiber reinforced composite with embedded Lithium-ion battery for its structural integrity concept. The comparison of versatile composite structures manufactured conventionally, air-sprayed and electrospun multiwalled carbon nanotubes in order to discover a better packaging method for incorporating lithium-ion batteries at its core is determined. In the electrospinning process recognized globally as a flexible and cost-effective method for generating continuous Nano filaments. It was incorporated exactly on the prepreg surface to obtain effective interfacial bonding and adhesion between the layers. The mechanical and physical properties of carbon fiber reinforced polymers (CFRP) with electrospun multiwalled carbon nano tubes (CNTs) have evidenced to possess higher mechanical strength incorporated between the layers of the composite prepreg than the traditional CFRP prepreg composite, At the same time the air sprayed CFRP with CNTs offers mechanical strength more than the traditional CFRP prepreg but lesser than the electrospun. This can be a design consideration from the economic feasibility viewpoint. They also contribute to efficient load transfer and structural load bearing implementation without compromising the chemistry of battery. The design validation, manufacture methods, and experimental characterization (mechano-electrical) of Multifunctional energy storage composites (MESCs) are examined. Experimental results on the electrochemical characterization reveal that the MESCs show comparable performance to the standard lithium-ion pouch cells without any external packaging and not under any loading requirements. The mechanical performance of the MESC cells especially electrospun CFRP is evaluated from three-point bending tests with the results demonstrating significant mechanical strength and stiffness compared to traditional pouch cells and conventional, air-sprayed CFRP and at lowered packaging weight and thickness. This mechanical robustness of the MESCs enable them to be manufactured as energy-storage devices for electric vehicles.

1. INTRODUCTION

1.1 Problem Statement

The Predominant design of Contemporary Li-ion batteries is for highest energy storage performance which also results in minimal mechanical load carrying capacities and strength. The construction of Li-ion pouch cells consists of alternating cathode and anode layers stack which are divided by thin micro-porous polymer membranes of separator. The sophisticated thin paper electrode films are comprised of copper and aluminum which have high structural composition. They are loosely stacked current collectors, which lead to less significant load transfer and mechanical linking between the individual layers. When these pouch cells are subjected to bending the exertion of least mechanical load causes unwarranted deformation and also leads to slippage between the layers. The packaging material is vacuum-sealed aluminum-polymer-laminate. Hence, the strength of the structure is minimal. The purpose of this study is to synergistically syndicate the load-bearing performances of current battery elements to assemble mechanical robustness to cells which would show huge savings in volume and weight of the packaging [1], [2] . In this study structural load-bearing batteries fabrication with the introduction of multifunctional energy storage composites (MESC) as an alternate strategy is performed. MESCs provide a novel form of energy storage system which offer quite the mechanical strength at less weight and provide excellent energy storage capabilities. The construction of MESCs is an integrated technique of embedding Li-ion battery electrode materials in advanced strength CFRP composites. In this approach there is no need in the electrochemistry modification of Li-ion batteries and can be adapted into standard industry designs, which are crucial for engineering implementation. There is significant increase in the moment of inertia of the laminate, with increase in greater flexural rigidity due to the sandwich-style construction [3]–[5].

1.2 Literature Review

1.2.1 Composite Materials: Overview

The physical and mechanical properties of the discontinuous fiber support are used to deduce the composite's key construction qualities. These are the composites' fiber-dominated characteristics. These are the fiber-controlled properties of the composites. However, in this discussion, the composites of interest are engineered, man-made materials with superior quality and stiffness relative to weight that are employed in high-performance structural applications due to these features. The fibrous support material is commonly described to as the discontinuous stage, whereas the matrix material is referred to as the persistent stage. The narrower meaning of composites is further apparent, and it can be limited to materials mixtures that feature high-fiber strength reinforcements supported by an elite matrix material. The matrix works as an adhesive binder for the fibers, providing support under compressive loads as well as shear abilities in two-dimensional lay-ups of fiber. It also transmits load within the stacks of composite, which include the load-bearing heap of composite materials. The mechanical and real qualities of fiber reinforcement discontinuous phase dominate the main designing properties. The matrix resists delamination and impact damage in two-dimensional composites. Matrix materials can be selected from a diverse spectrum of ceramic, and organic resin and materials. Except for the ceramic matrix, that may not be as stiff in comparison to the discontinuous fiber material. The expansion of small amounts of rubber base is often used to test the consistency of a variety of organic resin compositions. As a result, a discontinuous phase of particles is enclosed inside the composite's consistent phase of matrix. Fiber reinforced types of composites are classified according to the frame of the fibrous reinforcing material, with continuous, and discontinuous (short or long). The types of reinforcement, namely knitted, unwoven, woven, and orthogonal clusters of reinforcements, complicate the direct categorization. All the above are feasible, and each one offers an exclusive set of engineering characteristics. Fiber orientation, length and volume division are the levels of designing properties that are accessible. Continuous and lengthy irregular fiber-reinforced composites provide the most extreme levels of fiber property interpretation into useful composite qualities. The characteristics deteriorate as the

fiber length decreases. Fiber-reinforced composites (Continuous) are often made using a ply-to-ply lay-up approach that results in a layered laminar structure that may be switched out, to a three-dimensional composite, either lately or following impregnation with the matrix, although before cure and solidification [6].

High-performance composites provide a range of design qualities that are not possible to achieve with homogeneous metallic alloy structural materials like aluminum, steel, or titanium, and may offer a higher level of these properties. Most structural composites are used in mechanical, aviation, commercial, and military applications in the highest volume of resin matrix fiber reinforced composites. The US Air Force Materials Research facility developed high-performance composite materials in an effort to find structural materials that appear to be lighter than traditional materials. This massive and thorough R and D initiative to build composites occurred in response to a widespread need from the aviation community for basic materials that appear to reduce erosion and fatigue difficulties and save weight in airplane components. Fiberglass reinforced composites which are resin base have been successfully used in filament wound rocket engine cases, in addition to a variety of other aviation applications. Fiberglass reinforced composites lacked the rigidity required in high-performance structural applications such as airplanes, spacecraft, and missiles. The quest for greater modulus glass fibers yielded mixed results; nonetheless, the usage of boron, graphite, carbon and additional combinations developed in a creative breakthrough that created an untapped structural materials class known to be advanced composites. Further recent advancements have headed to the commercial accessibility of a broad range of high-quality, high-strength fiber materials, natural and synthetic, for use in high-functioning composite applications.

Highly developed composite material, although extra costly as a raw material, further difficult to plan with, harder to characterize, more expensive to make and collect, and more difficult to investigate in comparison to traditional primary metallic materials, have a scope in a large market such as sporting and military applications. Polymer matrix composites have found widespread use in a variety of fields where cost is less important when it comes to performance. Wearing and athletic applications such as shafts of golf club, casting poles, and skis have created a large industry and will remain to do so in the future [6].

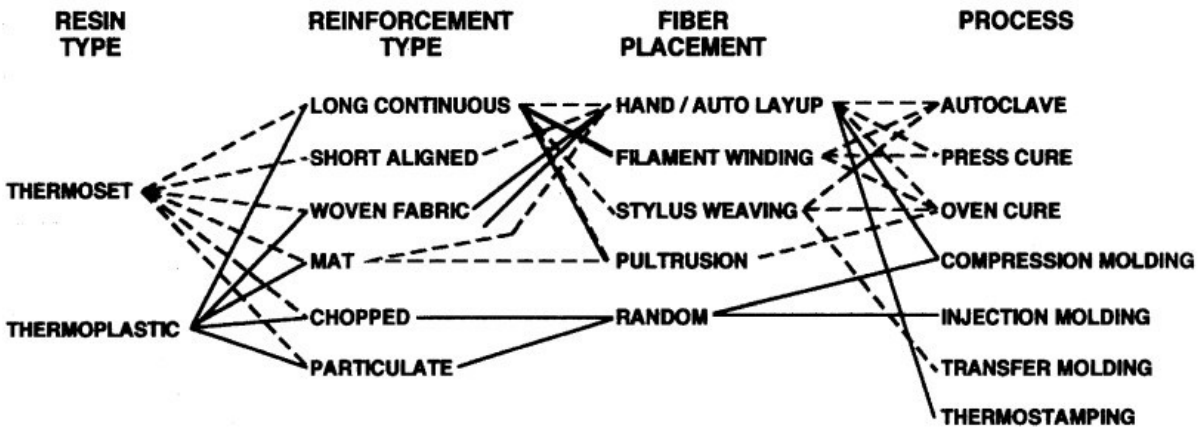

Figure 1.1. Composite Constituent Materials And Manufacturing Selections [7]

1.2.2 Classification of Composite Materials

The primary classification of composite materials can be made into the distribution of their constituents and by their form. There can be fibrous or particulate reinforcement. They are categorized as long or continuous fibers and short or discontinuous fibers. This orientation of fibers determines the mechanical properties of composites which are constituted to a range from anisotropy to quasi-isotropy properties. The second important classification is particle reinforced composite materials which vary in different shapes like platelet, spherical or any random geometry. Here the properties of composites are homogenous and isotropic [7].

Fiber Reinforced Polymers (FRPs)

The three prominent types of fibers are Aramid, Carbon and Fiberglass. Carbon fibers are applied to reinforce certain matrix materials, which are usually unidirectional to provide enhanced properties in a single direction. Glass fibers are reinforced to polymer matrix composites which provide anticorrosion properties to the finished product at low cost and improved strength. Kevlar fibers represents the group of aromatic aramid fibers. They possess excellent strength to weight ratio at lowest specific gravity.

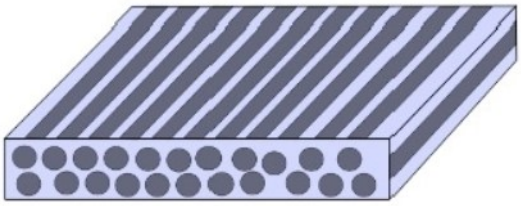

Figure 1.2. Fiber Reinforced Polymers (FRPs)

Ceramic Matrix Composites (CMCs)

The application of aluminosilicate, alumina, and calcium in reinforcement by silicon carbide is termed as ceramic matrix composites. They provide high service temperature limits, high tensile strength, hardness, and low density. As they are naturally resistant to higher temperature, they are more prone to fracture and brittleness. They are subdivided into four more classes: glass (alumina silicates and borosilicate), conventional ceramics (silicon carbide, aluminum or zirconium oxide, silicon nitride), cement and concreted carbon components [8].

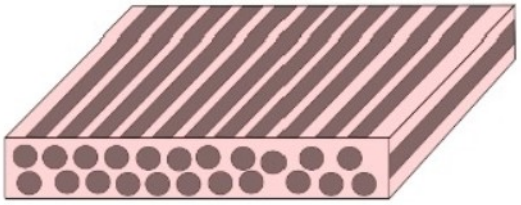

Figure 1.3. Ceramic Matrix Composites (CMCs) Diagram

Metal Matrix Composites(MMCs)

Like the name indicates these composites have metal matrix. Aluminum, titanium, and magnesium are the matrixes in these composites. To improve the design the metals are reinforced with carbon and silicon carbide fibers. The elastic strength and stiffness are increased in large folds due to reinforcements. This also aids in reduction of thermal and electrical conductivities, and large co-efficient of thermal expansion of metals [8].

Figure 1.4. Metal Matrix Composites (MMCs)

Sandwich Structure Composites (SSCs)

The core of a sandwich structure is constructed out of any architecture and mainly falls into 4 categories: foam or solid core, web core, honeycomb, truss core. This type of construction enables the core to resist transverse shear loads and the faces carries both in-plane and bending and keeps itself in place. They perform a significant role in all structural applications due to their high-level flexural ratio of stiffness-to-weight. They possess superior natural frequencies, buckling resistance, and lower lateral deformations [8].

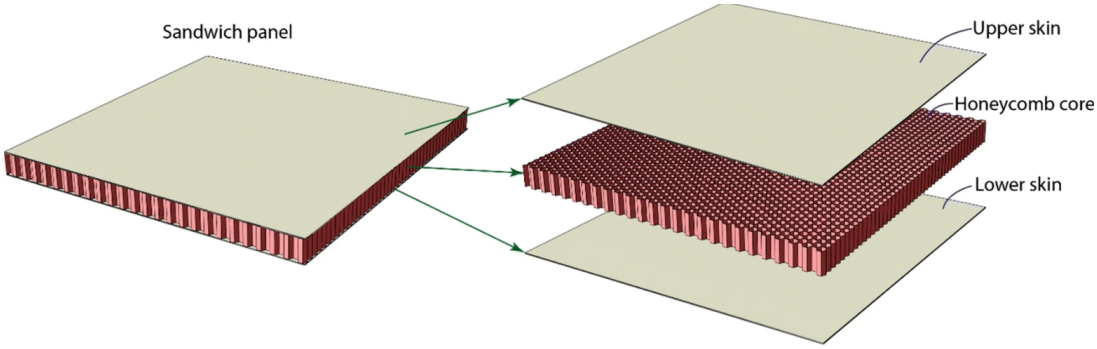

Figure 1.5. Sandwich Structure Composites (SSCs)

Laminates

The process of obtaining an excellent composite with increased durability and strength by stacking of varied materials is lamination. The iterations to obtain myriad of original materials in a desirable product is imperative in this process.

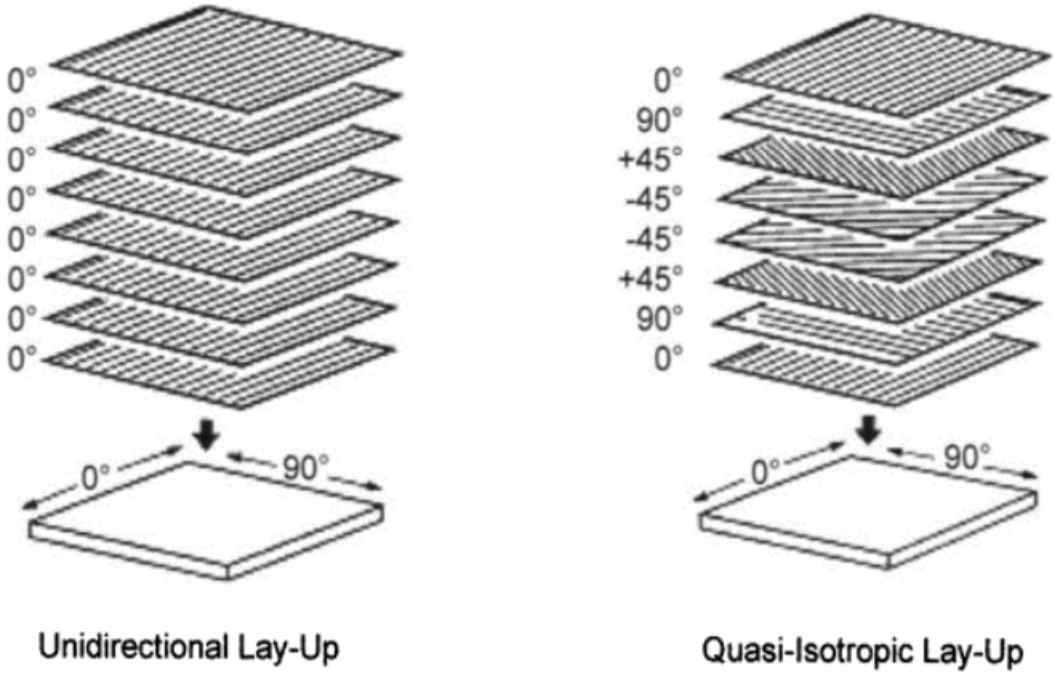

Figure 1.6. Laminates

1.2.3 Properties of Composite Materials

High Strength with Respect to Weight

The strength of the fiber composites is acute for the given weight. Various characteristics can be augmented by twitching the laminates. Chopped laminate provides comparable flexibility than the ply. The stiffness is another factor for consideration and should not be confused for strength. As the stiffness of the fiber composites is in many times fold greater than the mild steel of same thickness and has an ultimate strength to less than quarter of its weight.

Fire Resistance

The ever-escalating development in the recent years has expanded the properties of composites in two main areas have being: fire retardant and fire resistant. The application of chlorinated resins and additives like antimony trioxide on the laminates make it self-

extinguishing, meaning that they release Carbon dioxide upon burning and so when the flame cause is eliminated, it self-extinguishes. Application of phenolic resins in laminates allows for fire resistance. On the other hand, this process is tough to utilize as laminates are treated with formaldehyde and require a high degree of post curing to acquire real fire resistance.

Chemical and Weathering Resistance

The wide range of composite products resist the attack of versatile chemicals and have good weathering properties. The use of resins is the deciding factor in manufacturing of such laminates. The applications are in a wide variety of manufacturing of chemical storage links, pipes, chimneys and ducts, boat hulls and vehicles.

Low Thermal Conductivity

The application of Fiberglass in food storage industries, especially in the production of dedicated meat containers which maintain the prime cuts of frozen meat at lower temperatures for the purpose of exports in on demand currently. RTM process with special reinforcements and foam inserts is helpful here.

1.2.4 Ply-Orientation of Different Laminate Types

Symmetrical Laminates

The in-plane deformations in case of symmetric laminates are uncoupled from bending, i.e. [B] = 0. The classical lamination theory equation is [9]:

$$\begin{Bmatrix} N \\ M \end{Bmatrix} = \begin{bmatrix} A & 0 \\ 0 & D \end{bmatrix} \begin{Bmatrix} \epsilon^0 \\ K \end{Bmatrix} \leftrightarrow [A]\{\epsilon^0\}^{\{M\}} = [D]\{K\}$$

and

$$\begin{Bmatrix} \epsilon^0 \\ K \end{Bmatrix} = \begin{bmatrix} A^{-1} & 0 \\ 0 & D^{-1} \end{bmatrix} \begin{Bmatrix} N \\ M \end{Bmatrix} \leftrightarrow [A^{-1}]\{N\}^{\{K\}} = [D^{-1}]\{M\}$$

Specially Orthotropic Laminates

When there is zero coupling amongst in-plane extensions and shear deformation because of specially designated orthotropic laminates along with A16 = A26 = 0. The description is only related to the in-plane response and may not certainly mean that D16 = D26 = 0.

Cross-ply Laminates

The fiber orientations of 0∘and 90∘are distinctively composed cross-ply laminates. Independent thickness and stacking sequence for such orientations is $Q_{16} = Q_{26} = 0$, for such laminates are specifically orthotropic at $A_{16} = A_{26} = 0$. This also validates that $D_{16} = D_{26}$ $= 0$ [9].

$$[A] = 2t \begin{Bmatrix} n_1Q_{11} + n_2Q_{22} & (n_1 + n_2)Q_{12} & 0 \\ (n_1 + n_2)Q_{12} & n_2Q_{11} + n_2Q22 & 0 \\ 0 & 0 & (n_1 + n_2)Q_66 \end{Bmatrix}$$

Angle-ply Laminates

The fiber orientations with equal quantity of laminae at + and - and equivalent thickness are angle-ply laminates. Angle-ply laminates are orthotropic [9].

$$[A] = h \begin{Bmatrix} n_1\bar{Q}_{11} + n_2\bar{Q}_{22} & (n_1 + n_2)\bar{Q}_{12} & 0 \\ (n_1 + n_2)\bar{Q}_{12} & n_2\bar{Q}_{11} + n_2\bar{Q}22 & 0 \\ 0 & 0 & (n_1 + n_2)\bar{Q}_{66}(\theta) \end{Bmatrix}$$

Balanced-ply Laminates

The positive angles laminae are well-adjusted by equal negative angles laminae in a balanced laminate. These contain several pairs of balanced laminates like 0o and 90¬¬o on the reverse to the angle-ply laminates that are limited to a single set of matched angles. $A_{16} = A_{26} = 0$ and $D_{16} \neq 0 \quad D_{26} \neq 0$ [9].

Quasi-isotropic Laminates

Quasi-isotropic laminates demonstrate in-plane isotropic elastic response and are considered an imperative group of laminates. This includes 2N (N > 2) laminate which are symmetric and are of similar thickness. The N equal angles for this fiber orientations ($\triangle\theta = \boldsymbol{\pi}/N$), i.e., $\triangle\theta = 60°$ for N = 3, $\triangle\theta = 45°$ for N = 4, $\triangle\theta = 30°$ for N = 6 and so on. The reduced form for proving the in-plane stiffness and extensional matrix for quasi-isotropic laminates is

$$[A] = h \begin{bmatrix} U_1 & U_4 & 0 \\ U_4 & U_1 & 0 \\ 0 & 0 & U_5 \end{bmatrix}$$

where U_1, U_4 and U_5 are in-variants and h is the total thickness [9]

$$U_1 = \frac{3Q_{11} + 3Q_{22} + 2Q_{12} + 4Q_{66}}{8}$$

$$U_4 = \frac{Q_{11} + Q_{22} + 6Q_{12} - 4Q_{66}}{8}$$

$$U_5 = \frac{Q_{11} + Q_{22} + 2Q_{12} + 4Q_{66}}{8}$$

They are quasi-isotropic due to bending response of these laminates not being isotropic. Since $A_{16} = A_{26} = 0$, these laminates are orthotropic. There is no shear response and coupling in between these laminates [9].

1.2.5 Carbon Nano Tubes

The invention of multi-walled carbon nanotubes (MWCNTs) was through arc vaporization of graphite within an inert atmosphere of helium. The characterization of CNTs is based on two types: single-walled carbon nano tubes (SWCNTs) and MWCNTs. The only layer of graphene rolled with a smooth cylinder is the SWCNTs. Although two or additional concentric cylindrical shells of graphene layers which are coaxially placed over a main cavity core are MWCNTs. The SWCNTs are further categorized by zigzag, armchair, and chiral types according to the hexagons that are positioned in their structures. A multitude of research endeavors have been made to identify the structure-property relationships and the valuable purposes of polymer nanocomposite since its inception. Excellent mechanical, physical and functional properties along with exceedingly elevated aspect ratios give the CNTs the recognition of a potential reinforcement of polymeric materials. The CNTs are further explored into functional composites and structural composites. The exceptional properties of CNTs in the areas of thermal conductivities, opto-electronic beside mechanical properties are employed to progress multi-functional composites for submissions in the field of chemical sensing, electrical, thermal management, heat resistance, and photoemission [10].

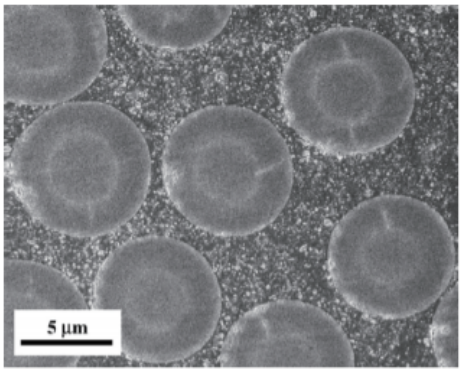

Figure 1.7. SEM Of A Multiscale CNT-CFRP Composite [10]

Nevertheless, the experimental investigation of the determined mechanical properties of carbon nanotubes composites have yielded faraway beneath their theoretical projected potentials, owing to several subjects like the non-uniform dispersion, breaking of CNTs during

processing and random nature of dispersion of CNT. Integration of CNTs into the three-phase multiscale composites depends strongly on how the properties of it are exploited on nanoscale. The modification consists of reinforcements in a common polymer matrix through either matrix or resin and the fiber reinforcements in the CNTs. An industrial compatible model is achieved by dispersing CNTs in the polymers by modifying the matrix resin. The validation of this process is displayed on scanning electron microscope (SEM) image. The different techniques employed for achieving CNT dispersion in matrix of polymer is by shear mixing, extrusion, calendaring, ball milling and ultrasonication. The major limitation to this method is the viscosity of the modified CNT matrix boosts exponentially with rising CNT concentration. The conventional composite manufacturing techniques cannot process extremely viscous CNT-agglomerated systems of resin. The best example to explain this is making multi-scale FRPs utilizing the vacuum assisted resin transfer molding process (VARTM), where nanofibers are sorted and result in heterogenous microstructure of multi-scale composites[10].

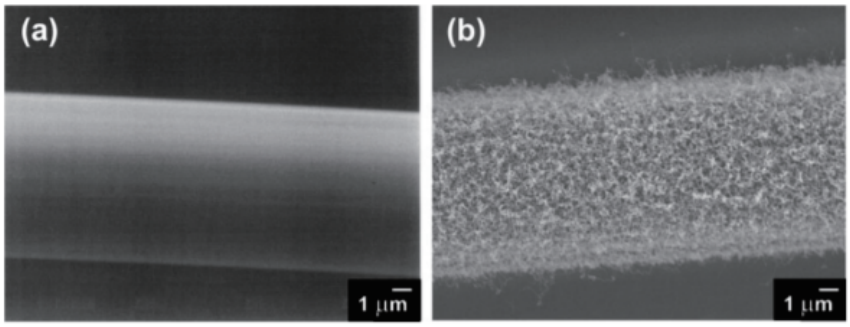

Figure 1.8. SEM Images Of Carbon Fibers (A) Before And (B) After CNT Growth [10]

1.2.6 Impact Damage Resistance of CNT-FRP Composites

The wide areas of applications in the field of aerospace and military limit the composite materials in terms of damage resulting from impact events. In this scenario the low-energy impact produces sub-surface delamination and has no visible surface damage, whereas the high-energy impact loading causes complete penetration and is detected on the surface. The substantial degradation in the mechanical properties was investigated through the internal

damage caused over periodic loading. The stiffness and in-plane strength were also affected by it. In composite laminates the failure mechanisms exposed to impact loading are mixture of energy concentration mechanisms like delamination affected from mode shear, transverse shear affected by matrix cracking and fiber fracture. The several factors like environmental conditions, loading, impactor geometries dictate the above fracture processes. Specifically, the interface properties of fiber and matrix, failure strains, and fiber configuration fall under material variables and are important to determine the damage tolerance and force loss resistance of the composite laminates. The research on inclusion of nanotechnology pointed towards enhancing this crash destruction resistance and tolerance is significant by the addition of nanofillers like nanoclay [10].

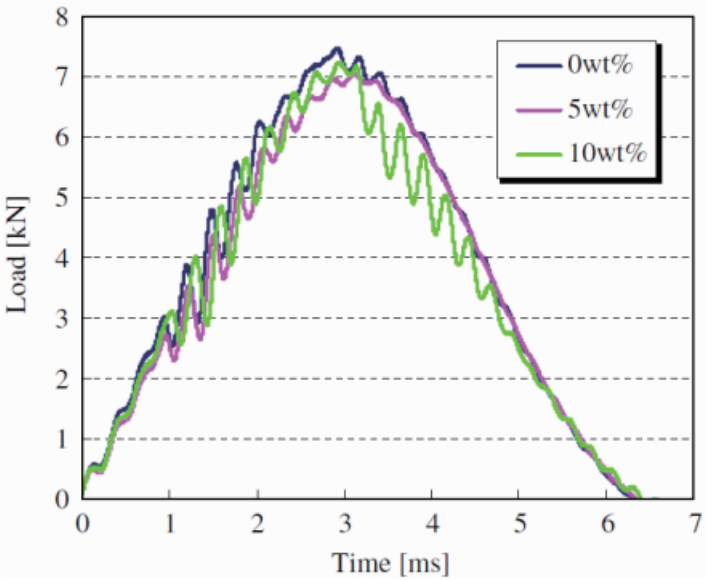

Figure 1.9. Time Vs Applied Load During Impact Test Of Multiscale CFRP Composites With 0, 5, 10 wt.% Cup-Stacked CNTs In Epoxy Matrix [11]

1.2.7 Electrospinning of CNT Composite Fibres

The modern application of electric fields to generate fine fibers which are nanometers in diameters is termed as electrospinning. They find a wider usage in filtration systems, medical devices, composite materials and membranes. Between the years 1964 to 1969 Sir Taylor engendered the electrospinning theoretically. This hypothetical procedure to affect the

droplet of water through electrostatic field get hopper and cone shape and the droplet squeeze out from the hopper head. This was first electrospraying method that can be considered as electrospinning. High-voltage power is supplied to the raw materials for electrospinning to improve the liquid electrostatic potential. The inter-molecular reaction of polymers makes them essential part of the raw materials of the process. The increase and decrease in liquid surface charge and electrostatic potential are an immediate link and so the same action will happen to the latter. The volume shape of the liquid is removed by the surface tension. The surface charge performs in the opposite direction to surface tension when the fluid is charged causing the fluid to change the shape and a structure is formed known as the Taylor cone. There is a constant challenge to the electrospinning process as their various parameters influential to the fibers.

Carbon nano tubes (CNT) possess a variety of mechanical properties like high modulus and high tensile strength but are a limitation when they are used as reinforcement in composite. This type of nanomaterials cannot envisage the desired mechanical properties. So, to integrate the nanotubes in the polymer nano fibers is a challenge to make the method of electrospinning it. Based on opposite conductivity the electrospinning process is anticipated to thread the CNTs end to end of the fibers of polymer dispersion and shear force. The fiber conductivity rises and the carbon sheets arrangement in electrospun nano fibers is fabricated. An electrical infiltration threshold of 2 wt.% MWCNTs show electrical conductance measurement on electrospun nanofibers [12].

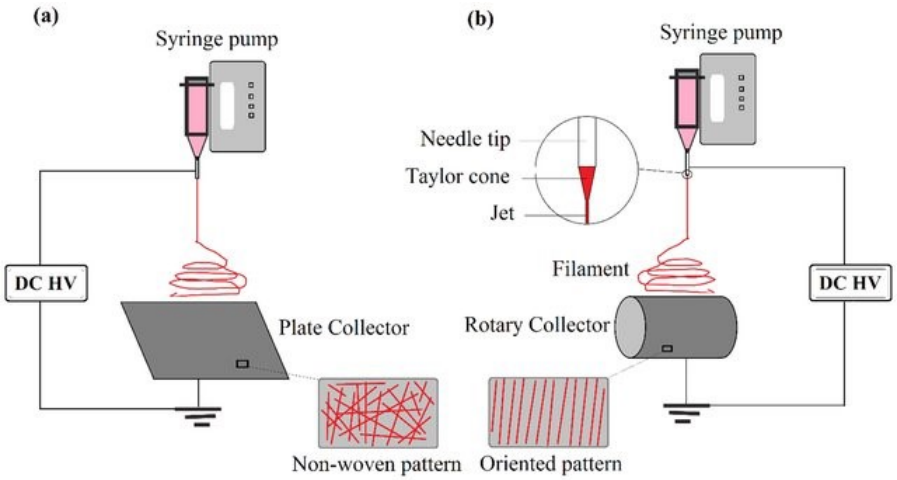

Figure 1.10. Electrospinning Methods [13]

1.2.8 Energy Storage Systems

Energy Storage Systems have undergone continual upgrades to attain their current versions of development for centuries. This is stable for many types of storage. Several categories of storage devices occur and are labeled in quite a number of ways. 'Ragone plot' is a technique to represent the specific power and energy of storage characteristics in types of electrochemical energy storage. It helps to detect the potentials of every storage kind and differentiate for fluctuating energy storage capabilities with on-demand power extraction prices. The plot additionally benefits in choosing the highly excellent power storage for certain needs or applications. The storage energy density is defined as the strength accrued per-unit mass or volume, and power density is defined as the per unit mass or volume energy transfer rate. The produced power is no longer accessible for a longer period, then storing large quantities of energy is needed in a high energy density device. Similarly, a high-power density device is needed for devices along with charge or discharge variations within a short time. Based on storage period, energy storage systems additionally can be categorized. Shorter duration energy storage entails the storage strength up to a period of days, whereas long duration storage implies to the storage of strength to a year [14].

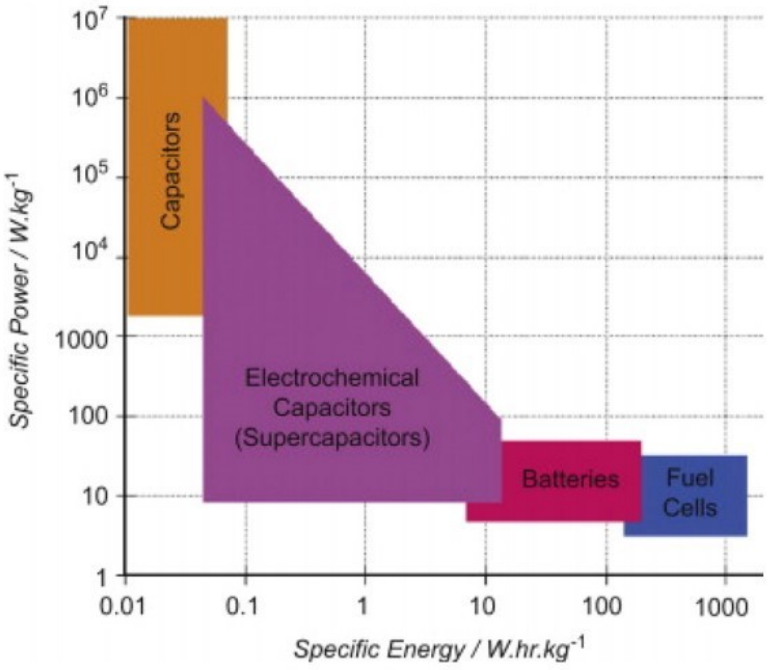

Figure 1.11. Plot of Energy Storage Ragone [15]

The general layout of an energy storage resource contains a storage form, a power transformation system, and a stability system. The several types of energy storage are classified as electrochemical and battery, flywheel and thermal, thermochemical, compressed air energy storage, magnetic, pumped, hydrogen, and chemical energy storage. This discussion is focused on electrical energy storage (EES). This is described as a method of translating electrical energy from a power system into such a form which can be collected to, by translating to electrical energy. This permits electricity to be made at conditions of lower order, or from sporadic energy resources and low generation cost to implement at the time of elevated generation cost and requirement or when there is no means of production available. The applications include stationary energy resources, transportation vehicles, portable devices. The development record of EES dates to earlier 20th century as lead acid accumulators were used to supply residual loads on the direct network as power stations were often shutdown. The conventional electricity generation companies require EES's instantly. These companies have little to no storage facility, unlike many different commodities markets. The electrical energy transmission and circulation systems are conducted for straightforward one-way

transport from far off and massive strength vegetation to users. This implies that power should continuously be utilized absolutely once delivered. In any case, the request for power shifts impressively emergently, every day and regularly, the most extreme request may as it was final for some hours once a year. This indicates to unproductive, over-designed, and high-priced factories. EES approves energy manufacturing to be de-coupled from its source, self-created, or purchased. This is imperative to large generation systems who require to create necessary producing capacity to gather median electrical demand instead of higher needs. Here EES provides substantial merits which includes peaking power and standby reserve. This raises the remaining productivity of thermal power sources and reduce toxic emissions [16], [17].

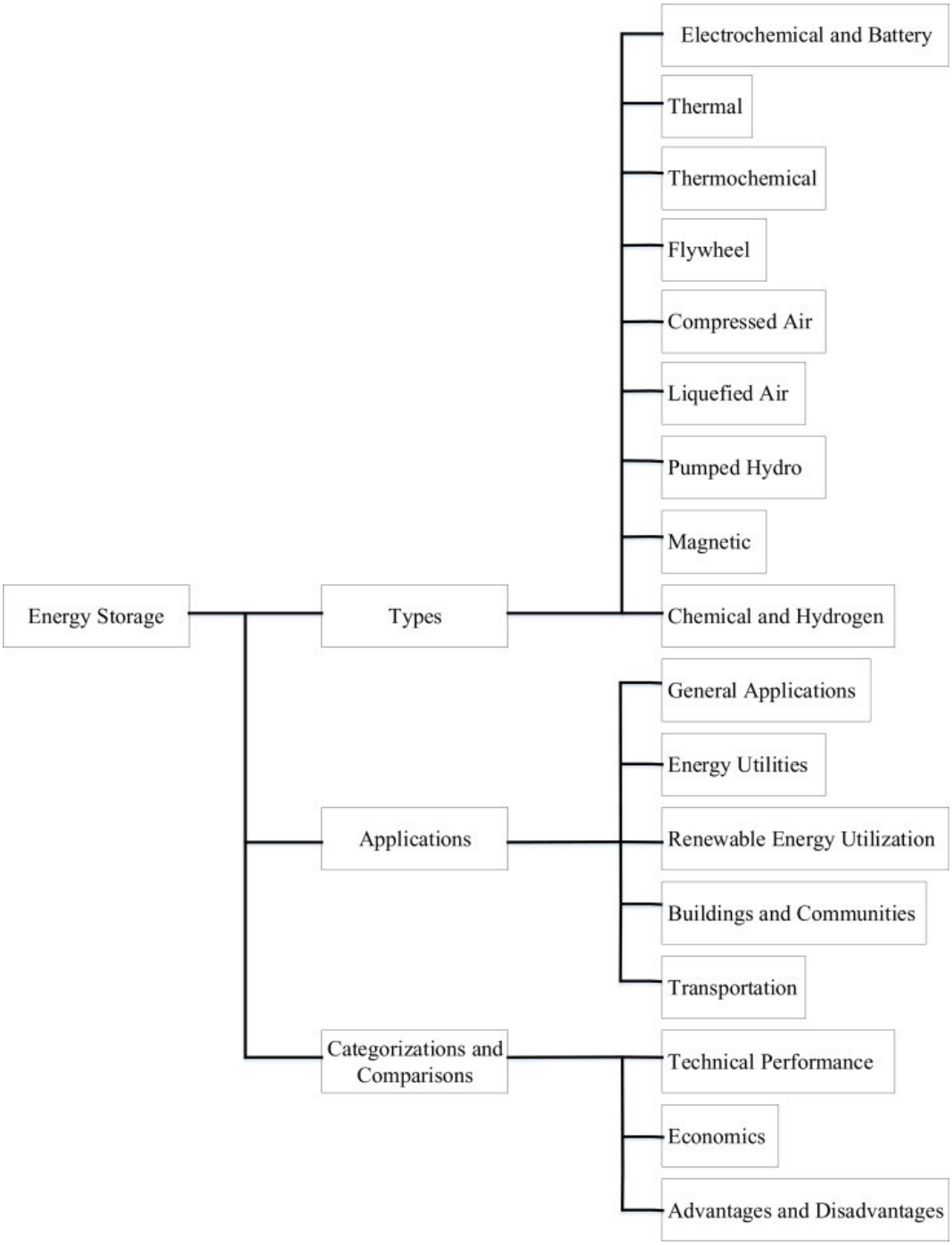

Figure 1.12. Categorization Of Energy Storage Systems [16]

1.2.9 Damage Evolution in Pouch Cell Subjected to Indentation Loads

The application of batteries in electric vehicles poses a safety concern when subjected to crash. The high energy density of the lithium-ion batteries is the responsible factor in this scenario. During the crash, the several deformations suffered by the battery pack can cause an internal short circuit and leads to explosion and fires. The analysis of fracture mechanism and battery deformation improves the crash worthiness of the battery systems. There is lack of research on study of existence of inside short circuit of battery cell in numerous mechanical loads. Several simulations have been carried to examine and envisage battery cell distortion and failure. Finite Element (FE) program is applied to investigate the relation among short circuit onset and mechanical behavior by means of two material models. Under quasi-static indentation loading this shows the global force-indentation responses of battery cells. Buckling distortion of the sandwich structure is captured by a comprehensive RVE model of a battery cell to examine the mechanical behavior of Li-Io batteries under in-plane compression. Uncontrolled thermal effects by conductive interaction among anode and cathode is the explicit source of internal short circuits of Li-Io batteries. The fracture in separator is the major factor for internal short circuits and have no effect on active materials failure criterion. It is highly likely that the active material layer undergone damage before the separator breakdown because of this brittleness. The simulation experimentation of the homogenized model to perform the indentation tests includes 3 kinds of pouch cells ranging from small user electronic cells to big size cells applied in electrical vehicles. The prediction findings suggested that the detailed failure progression in the multi-layer structure of battery cells in diverse loading suggest that the failure reason of separators varies on the stress state.

The testing of this study is initiated by an industrial Li-Io battery pouch cell. The anode is graphite and a Li (NixCo1- x-y Mny) O2 cathode. To display the surface morphology, the microstructure of the separator in battery cell is examined by using Scanning Electron Microscopy (SEM). The composition of the separator comprises of two layers: the upper and lower layer of ceramic coating facing the anode and wet-processed polyolefin film on the cathode side. The dimensions of pouch cell are 150 mm (width) and 250 mm (length) with the pouch cell thickness of 7.2 mm and separator thickness of 0.028 mm.

The voltage of the pouch cell is 3.7 V with a nominal capacity of 20 Ah. Universal testing machine is employed for the overall experimentation of Quasi-static depression assessments of the pouch cells. A curved punch head indenter of steel with 13.00 mm diameter electrically insulated by a Teflon block is employed on the mounting socket of test machine. The indenter goes vertically downwards at a velocity of 0.5 mm/min on the center of the pouch cell during the testing. A speckled pattern is involved in the duration of testing to evaluate the indentation trace link of the punch head on the side surface of the punch head. The movement of the punch head was taken by a digital CCD camera. The data processing enabled to calculate the indentation strokes by Digital Image Correlation. The study of deformed areas on the pouch cell were designed with interruptions on a cycle of indentation tests. The pouch cell is under loading from the indenter until the preset force is achieved and once it reaches the position the pouch cell is unloaded. Next, the cell is gently dismantled to evaluate the deformed regions and at each one stage the test is being reiterated twice [18]–[22].

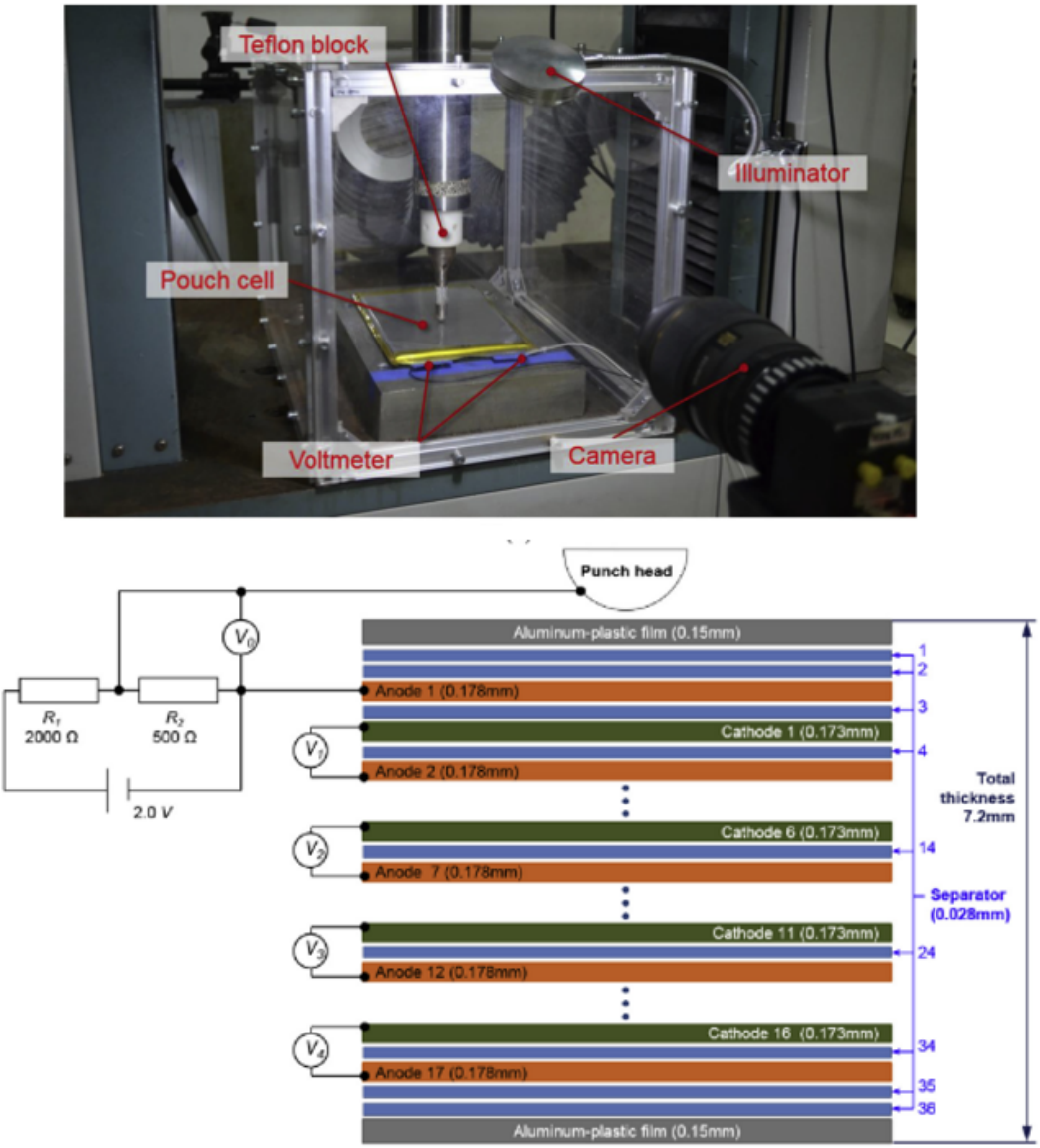

Figure 1.13. Setup of Loading And Measurement Pouch Cell Indentation: (Top) Setup of Test, And (Bottom) Composition, Thickness Distribution Of Pouch Cell And The Voltage Measurement Outline Of Fracture Sequence Analysis [19]

1.2.10 Multifunction Energy Storage Systems

Recently structural batteries are a trending concept emerging to overcome limitations of functionalities in load bearing to accomplish weight and volume reductions in several structural areas involving aircraft, spacecraft, and commercial vehicles. These structural

batteries are incorporated by energy storage functionality. The packaging material plays the imperative role of load carrying capacity in these existing batteries instead of the energy storage materials themselves. Many commercial industries are aiming to reduce the structural weight of their core products to curb greenhouse emissions. In this pursuit, carbon fiber composites are being gradually utilized in the structural parts of the motor vehicles like the body panels and chassis. As development moves towards electric propulsion with increase in demand for hybrid and electric vehicles in the market, challenges arise for the energy storage in these vehicles in regards of space in the vehicle. This also impacts on the empty weight of the vehicle as the battery system of the vehicle only weighs up to 25% of the total body weight. This creates a larger storage area in volume. Structural and space effectiveness of the vehicle utilization of multifunctional composites in vehicle components is necessary to enhance overall storage. There are various approaches to incorporate the electrical storage devices with structures of composite. The first being, fabrication of the composite in a structural dielectric capacitor (SDCs) [23], [24].

i. Multifunctional composites with embedded LiPo Batteries

Here the carbon fibers operate as the electrodes and additionally bear the load of the structure. This application can be a multifunctional material serving the composite material as an electrical energy storage device meaning, a battery. Secondly, use of multifunctional structures in the form of embedding the batteries within composite materials. In this way the composite structures provide the functionality of energy storage and load bearing. This is also a space saving method than other conventional batteries. The incorporation of batteries in composite materials to generate lightweight, energy storage structures are an encouraging methodology for the next generation of electric and hybrid automobiles. Multifunctional composite structures that merge elevated storage capacity with superior mechanical properties is also evaluated in ships, aircrafts, and spacecrafts. One such prominent energy storage is the Lithium Polymer Battery (Li-Po). They have higher energy density and the capability to preserve intermittent charging with fast charge-discharge rates. There are the justifications why Li-Po batteries are prevalent preference for energy storage in the electric

and hybrid vehicles. This embedding process requires a well understanding of the mechanical properties. There are several studies analyzed dynamic and mechanical properties of the laminates including the energy storage devices. The studies explored that the batteries sandwiched inside the composite materials undergo an increase in bending stiffness which decreases the failure stress. The escalation in bending stiffness was credited to the arithmetical stress concentration initiated with non-uniform thickness formed by the existence of an embedded battery, also the fragile interfacial link in the middle of the composite laminate and the battery. Other experiments demonstrated that batteries sandwiched in composites core have undesirable effects the in-plane compression properties. The vehicle modules are frequently exposed to static and dynamic compression loads, hence recognizing these effects of compressive stress loading on the mechanical properties of the laminates is critical in energy storage and the performance on the vehicle design [2], [25], [26].

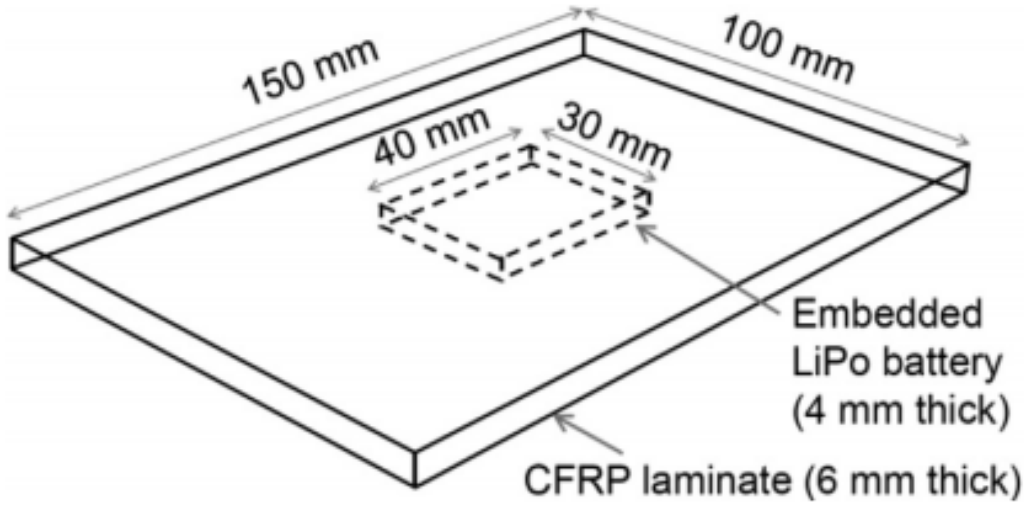

Figure 1.14. Carbon FRP laminate with an embedded LiPo battery Representation [27]

The failure stress, fatigue life and compression modulus of carbon-epoxy laminates decreases with insertion of LiPo batteries. This impregnation clearly into the material not only stores energy but also saves dimensions. The magnitude of cutback differs on the insertion of batteries relative to the direction of compression load. Stacking the batteries to play down the decrease within the load carrying range of composite material, which was in the

perpendicular direction, yielded in lowest decrease to the compressed properties. Stacking several batteries in the way of loading can end in better energy storage capacity and also save ample space compared to a single battery which is associated in the identical stacking sequence [27], [28].

ii. Multifunctional composites with embedded Li-Ion Batteries

A recent subject of several researchers for energy storage composite structures are thin film batteries. They have a dimension of 1 mm thickness and can be impregnated in the composite laminate without significant modification to the structural design. They can be formed into various complex shapes than the conventional pouch batteries, but they lack capacity. Composites with inserted TFBs have been manufactured employing CFRP prepregs and glass fibers fortified polymer (GFRP) prepregs. TFBs are ordinarily embedded between layers of prepreg fabric. They are sandwiched between layers of prepreg material and are attached to a solar cell by means of an inkjet printer. This sample is further unified with laminates. Then these laminates are cured at higher temperature and pressure. Application of adhesives to bond he laminates and TFBs is also complementary manufacturing technique. The applications include bonding of actuators, supercapacitors, flexible solar panels on a fiberglass substrate with two-part epoxy to develop an energy storage device. Alternative approach includes bonding several electronic layers on composite laminates. Aside from solar cells the TFBs are combined with piezoceramics to obtain self-charging composite structures.

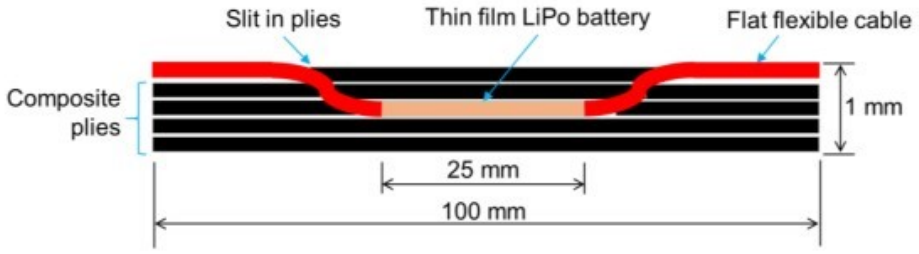

Figure 1.15. Energy Storage Composites Laminates with an Embedded TFB [29]

iii. Multifunctional composites with embedded Li-ion bicells

This construction is of three electrodes; a central anode which is sandwiched between two cathodes, and this can be built into energy storage composites via two approaches. The first method is a stack of bicells in aluminum packaging or CFRP laminates which is vacuum sealed. The second method employs stacked bicells at the heart of sandwich structure. They can be adhesively bonded to the laminates for manufacturing purposes.

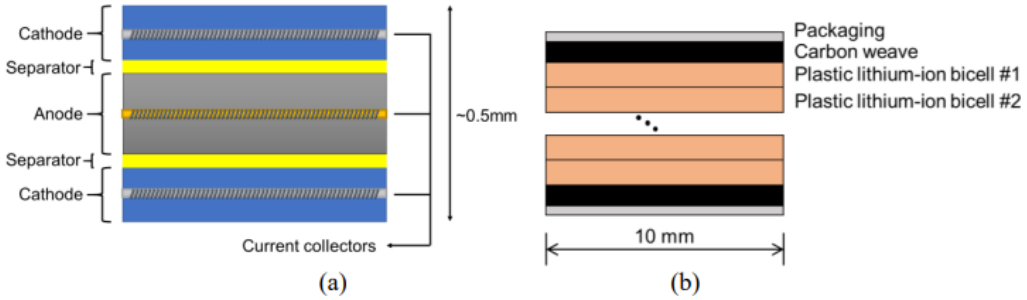

Figure 1.16. (a)Schematic of Li-Ion Bicells; (b)Li-Ion Bicells within a Carbon Weave Pouch

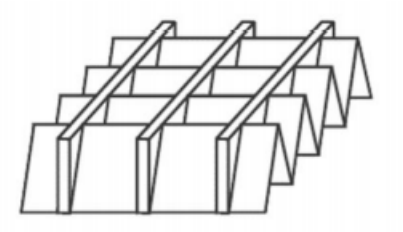

Figure 1.17. Vertical Bicells And Aluminum Triangular Corrugation Used In The Core Of A Sandwich Composite

1.2.11 Testing and Performance of Multi-functional Composite Structures

The composite structures undergo change in mechanical properties on insertion of batteries in them. However, the performance of these structures is suitable matched to those without an energy storage system. When it comes to electrical properties the composite structures safeguard the batteries when they are under mechanical loading and also aid in operating of the batteries while they are under loading.

i. Tensile test methods

Tensile tests are the means according to several ASTM protocols on the laminates and sandwich composites with implanted batteries. The different shapes and sizes of composites are considered for these tests like the dog bone shaped in this case. 135 mm and 36 mm is the gauge length. The end tabs of glass-epoxy laminate were connected by adhesive (Araldite) to its edges for the sample mounted in the loading machine. The samples were loaded to failure on a MTS universal testing machine having 250 kN capacity. The displacement rate was constant at 2 mm/min. During tensile testing, minimum of four coupons were analyzed under identical conditions the surface strain field of every sample was measured by digital image correlation (DIC) technique. The evaluation of DIC statistics was completed in MATLAB. There are three types of strain measurement: global strain where the average strain is over the entire gauge surface, local strain: the typical average strain over the gauge length width where the batteries are inserted and far field strain: the average strain over the gauge length width where there are no batteries These sum up to quantifying battery effect on worries to the strain of surface which is created under tensile loads [30].

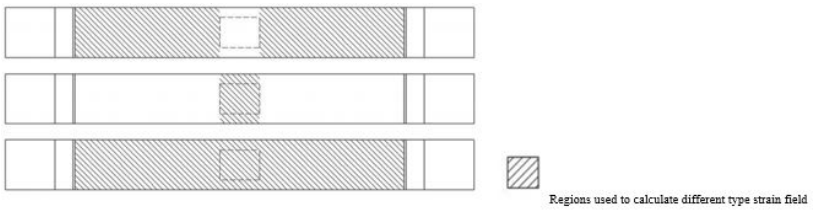

Figure 1.18. Sample Surface Representing The Areas Of (Top) Global, (Middle) Local And (Bottom) Far-Field Strain As Measured With DIC. Dashed Lines Show An Embedded Battery Location [30]

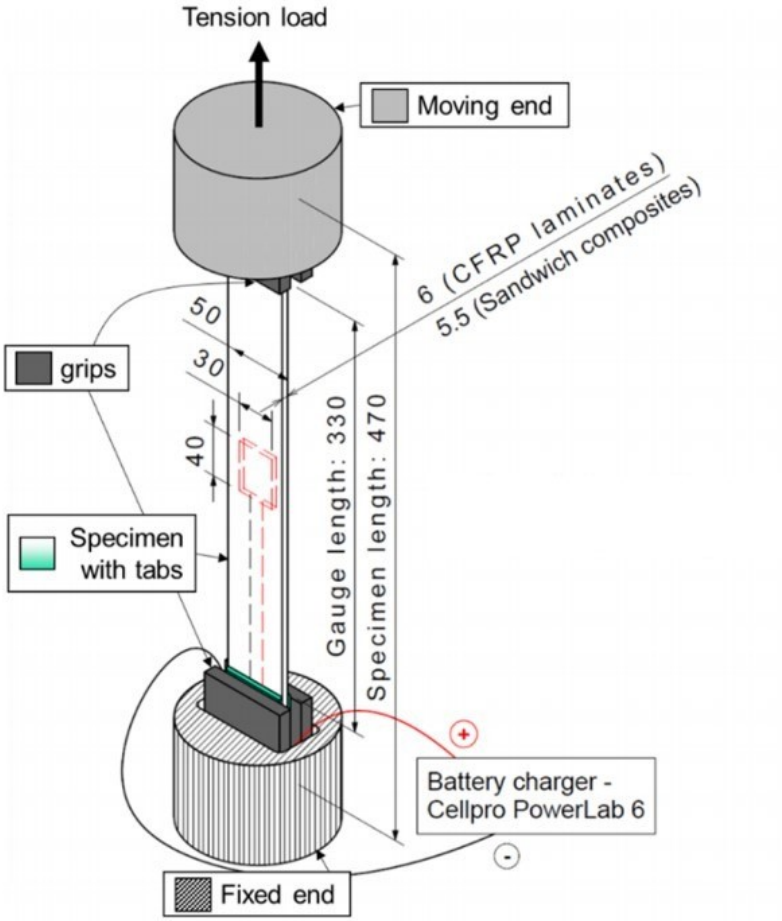

Figure 1.19. Schematic Of Experimental Tension Test [30]

ii. Compression Analysis

The compression testing on the laminate and battery specimens are conducted according to ASTM standards. The sample is on the warp tow direction loaded on the laminate of carbon fabric. Anti-buckling guides are utilized to eliminate the out of plane buckling of the sample and to ensure the material failure occurs inside the boundary of gauge area. The machine employed is an 0.5 mm/min end shortening rate 250kN MTS machine. The testing is conducted in a fume hood with fire extinguishers and containment equipment to alleviate the threats related to battery fire hazards triggered due to internal short circuits of cells. Application of sinusoidal load cycle results in compression-compression fatigue tests on the laminate specimens. The dimension of the specimen remains constant as in the case of

described for static testing. The loading frequency of 3 Hz at a R ratio of 0.1 until failure is specified. The failure is estimated by the failure of sample in bearing highest fatigue stress. In this case if the sample did not attain failure the test got halted on 106 cycles [31]. A specific number of laminate types were examined across a scale of highest fatigue values of stress to plot the curve of fatigue life.

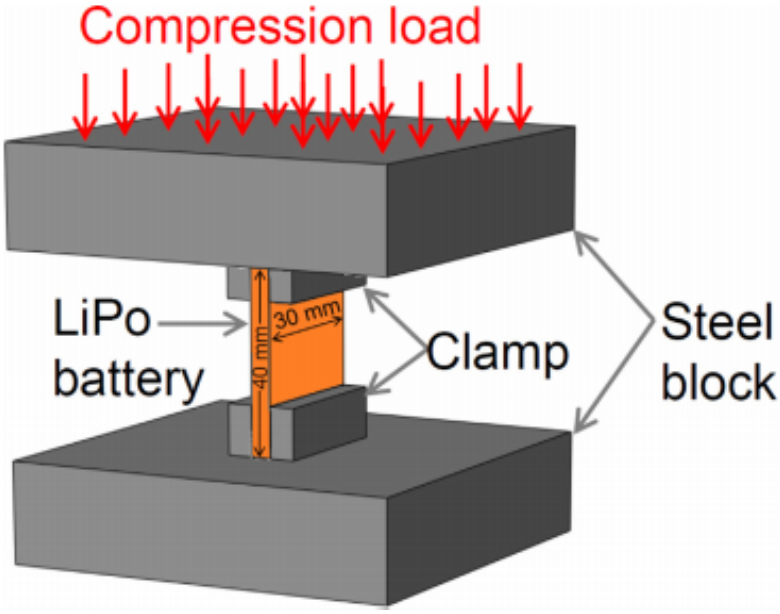

Figure 1.20. The Compression Test Conducted On The LiPo Battery [27]

To evaluate laminate surface for strains through duration of the fatigue and static compression testing, Digital Image Correlation (DIC) is implemented. A Digital camera is employed on shorter distance from the sample and a superior contrast arbitrary speckle pattern is put on the laminate surface prior to testing. The DIC images are then recorded during the testing. The images are then post processed to extract the strain values and displacement in MATLAB [32]. There are three types of strain values obtained in this process, the average strain over the complete sample known as Global strain. The region away from the battery with embedding is the average strain which is also known as the Far-filed strain. The location on embedded battery which is average strain is also known as the Maximum strain. Prior to, Through and next the Static testing and fatigue testing of the battery (electrical) performance is monitored. Cyclic charge/discharge was executed by employing Cellpro PowerLab

6 multi-chemistry workstation. The testing was carried out at room temperature under a constant 1C rate (500 mAh-1). The current, internal resistance, capacity and voltage of the batteries in cycling was evaluated at an interval of ten seconds. Same procedure of testing the electrical properties of the battery before embedded within the laminate and for the duration of the testing for compression is measured [27].

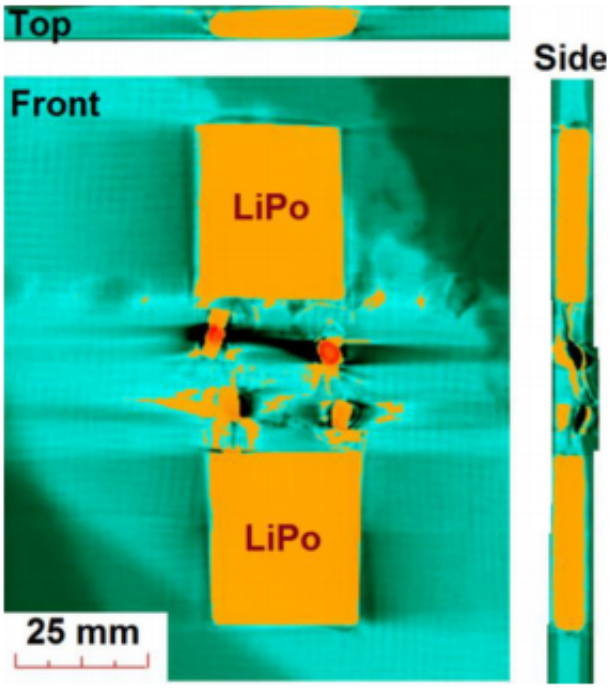

Figure 1.21. Cross-Section Views Of The Composite Laminate Displaying Vertically Arranged Two Embedded Batteries (X-Ray CT Image) [27]

iii. Vibration and acoustics analysis

Laser scanning Doppler vibrometry (LDV) is employed to measure sandwiched composite laminates for vibration and acoustic properties. This schematic representation includes a beam modeled sample to be horizontally held with strings on both ends from a fixed structure to present a free boundary condition. Excitation is generated from a mechanical shaker at a stationary point from one end of the sample. A non-perpetual thermoplastic adhesive is bonded to the shaker head of the specimen. The shaker end has a load cell connected to measure the input force. Frequency span from 0 to 2.5 kHz is applied to stimulate the sample

in a periodic chirp signal in an arbitrary abatement, at 3200 FFT lines through the bandwidth to offer a resolution of 0.78 Hz. The velocities, accelerations and out-of-plane displacements are recorded with a non-contact laser vibrometer at 69 equidistant scanning points in both transverse and longitudinal directions. The specimen is placed at a certain distance from the head of beam source for a full-filed view and a low pass filter is applied to eliminate the signal with high frequency blare. The frequency-velocity response curves yield first three modes of vibration, which are acquired by being in the region of the responses at 69 evaluation points. The first three modes of vibration also yield damping ratios of the specimen with use of 3 dB half-power bandwidth method. Wave-number amplitude and coincidence frequency are concluded for the specimens for acoustic analysis. The frequency at which vibrations become audible is termed coincidence frequency and is defined by evaluating the LDV data in the wavenumber domain. The wavenumber domain is transformed into a Fast Fourier transform along the center beam which is measured across at 23 equidistant points for measuring the frequency response function. Counter plots are extracted from the wavenumber-frequency response, once transformed into wavenumber domain [33].

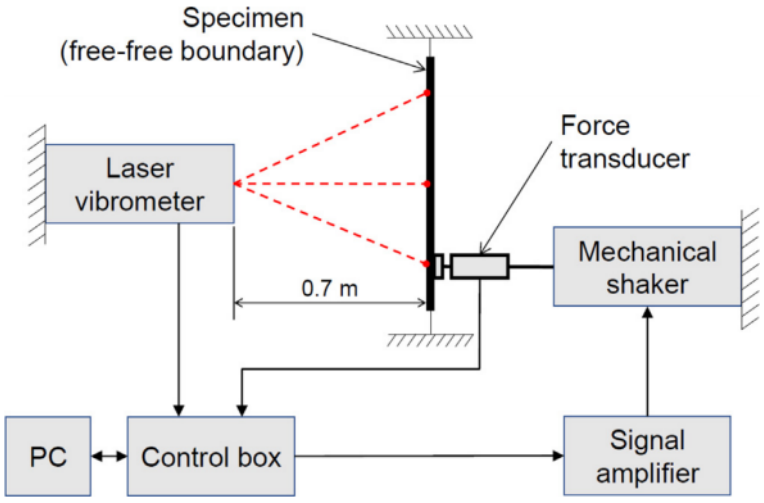

Figure 1.22. Laser Doppler Vibrometry Experiment Setup [33]

2. EXPERIMENTAL PROCEDURES

2.1 Air-spraying and Electrospinning Solution Preparation

In this study, for the purpose of fabrication of CFRP facesheets the solution preparation is the initial step. The method of application on the CFRP facesheets is the comparison factor, otherwise the solution remains constant. a masterbatch (MB) of non-functionalized multi walled CNTs which is made up of epoxy resin based upon Bisphenol A (50 - 99 pbw. %), and ethanol solvent (less than 15% volume), carbon nanotubes (4 wt.%) (Nanocyl™ S.A., Belgium) was used. The following is the procedure to prepare the 4 wt.% multiwalled CNT solution.

1. Measure the empty container weight and record.
2. 1.5gm of MB in 5ml of DMF (10 min. magnetic stirring without heat)
3. Probe sonication for 8-10 min. (10% Amp, 45 sec ON, 30 sec OFF)
4. Add Triton-x 0.075gm (1:20 =Triton-x: CNT)
5. 10 min. magnetic stirring without heat
6. Probe sonication for 8-10 min. (10% Amp, 45 sec ON, 30 sec OFF) [Step 2]
7. Add neat epoxy 1.5gm and 15-20 min magnetic stirring without heat
8. Probe sonication for 8-10 min. (10% Amp, 45 sec ON, 30 sec OFF) [Step 3]
9. Add hardener (1:15 = Hardener: total mixture)
10. 2 hrs. of magnetic stirring at 50° C heat
11. Degas in vacuum for 10-15 min. without heat
12. Resting period starts [34]

2.1.1 Electrospun CFRP Facesheets Sample Preparation

A MESC cell is comprised of the simplest form. Fundamental modules of it are the core battery, the structural facesheets and the adhesion that maintains the true form of the cell. In this research the design and analysis of the cell sample is a material optimization problem where material selection and geometric configuration of the facesheets allow a multitude assortment of probable electro-mechanical properties combination and is consistent with the load carrying performance of material in amenability to distortion under a three-point bending load. The electrospinning process of CFRP samples is similar to that of the conventional samples from the initiation of cutting the prepreg sheets and then laying it up. The electrospinning method of depositing MWCNTs/epoxy ENFs on the carbon fiber layers for the improved version of the composites. The procedure for making the Air-sprayed CFRP facesheets start with cutting of the prepreg sheet. A hot melt epoxy-carbon fiber which has a plain weave pattern (SE70 Gurit Holding AG, Wattwil/ Switzerland) with a balanced, symmetric, and asymmetric laminate (10 x 10 cm) stacks were manufactured. A hand layup method was applied and then vacuum bagging to reduce the void ratio. The stacking sequence on one side of the cell is [0/90/±45]2s. Square slots were cut before laying up in the stacking. A total of 20 layers had been used for making a single sample. The samples were vacuum bagged for a period of 60 minutes to achieve maximum adhesion between the layers before curing. The sample was completely cured by arranging them in a programmable oven (Easy Composite, UK) at 120°C for 25 minutes and vacuuming under 1 bar. While retaining the pressure, the samples were cooled down at ambient temperature. The samples were given a smooth finishing at the edges for appearance. The final thickness of the sample after the curing process was 0.52 cm and the thickness of the sample with thermoplastic sheet in the middle layer was 1.1 cm [34] [35] [36].

2.1.2 CFRP Facesheets Sample Preparation

The sample preparation was created according to two different dimensions and for testing of two characteristics in 3-point bending and tensile testing. The procedure started with cutting prepreg sheets in dimensions of (35 x 5 cm) stacks of 20 layers and (10 x 10 cm)

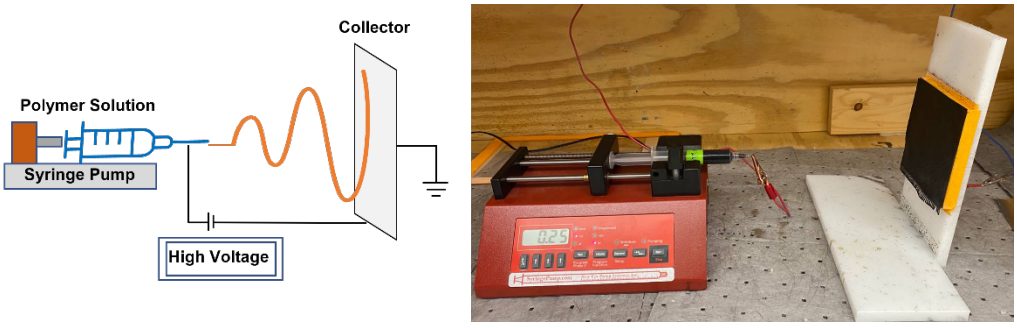

Figure 2.1. Electrospinning Schematic

stacks of 20 layers. A square slot for accommodating the battery was cut in both the samples of (6 x 4 cm). For tensile tested sample 2 slots were cut at 5 cm on both the sides. The epoxy-carbon fiber employed was (SE70 Gurit Holding AG, Wattwil/ Switzerland) with a balanced, symmetric, and asymmetric laminate of a plain weave pattern. The stacking sequence on one side of the cell is [0/90/$\pm$45]2s. The samples were laid on the plate for vacuum bagging in a sequence of 10 layers on each side to ease the manufacturing while assembling the cell. The samples were vacuum bagged for a period of 60 minutes to achieve maximum adhesion between the layers before curing. The sample was entirely cured by arranging them in a programmable oven (Easy Composite, UK) at 120°C for 25 minutes and vacuuming below 1 bar cooling them down at room temperature under same pressure.

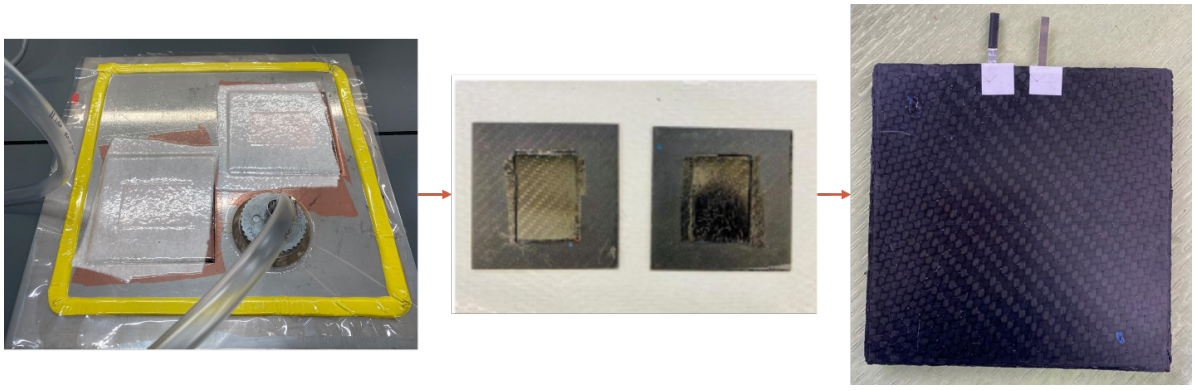

Figure 2.2. CFRP Structure Preparation

2.1.3 Air Sprayed CFRP Facesheets Sample Preparation

The procedure for making the Air-sprayed CFRP facesheets start with cutting of the prepreg sheet. A hot melt epoxy-carbon fiber which has a plain weave pattern (SE70 Gurit Holding AG, Wattwil/ Switzerland) with a balanced, symmetric, and asymmetric laminate (10 x 10 cm) stacks were manufactured. A hand layup method was applied and continued by vacuum bagging to lessen the void ratio. The stacking sequence on one side of the cell is [0/90/±45]2s. The 4 wt. % multiwalled CNT solution was then filled in the collector can on the air-spray gun. Each of the layer on both sides was then sprayed with the solution and then vacuum bagged individually with 10 layers on one side. The rectangular sample also followed the same procedure as above to get cured in the oven.

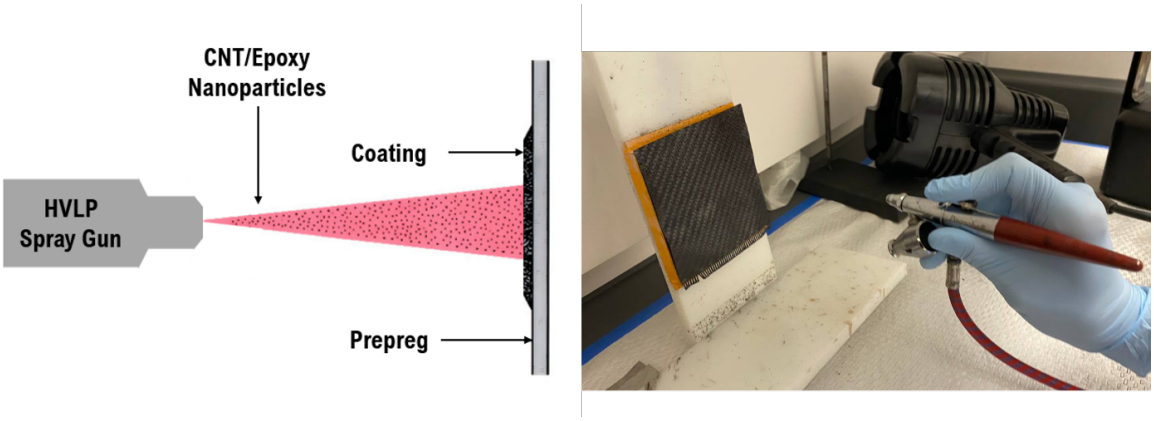

Figure 2.3. Air-Spray Sample Preparation

2.1.4 Assembly of the Batteries Inside the CFRP Samples

The fabrication method of the MESC cell was operated in a sequential manner. Two CFRP facesheets with the rectangular slot in the middle is placed flat on the surface. A prepreg sheet of the same dimensions with a same slot space is employed as the adhesion between the two surfaces. The edges of the two surfaces are heated at a temperature of 70°C by the means of a heat gun. The prepreg sheet is placed on one side of the CFRP face sheet and the pouch cell battery is placed at the center of the surface. Due to the heated surface, the epoxy in the uncured prepreg sheet enables it to act as an epoxy adhesive and both

the surfaces are then joined together. The sample is then compressed in a heated hydraulic press to melt further the epoxy resin in the middle layer of the sample and helps to fuse both the surfaces of the facesheets together securely (100°C, 0.5 MPa pressure). The sample remained to cool down to room temperature under the same temperature, at this stage the epoxy hardened and hence equilibrated the stack mechanically. Edges of the sample were then sealed off with additional epoxy adhesive for a tidier appearance and homogeneity of the two surfaces. This method was applied to produce six samples with three of symmetric orientation samples and three of asymmetric orientation samples.

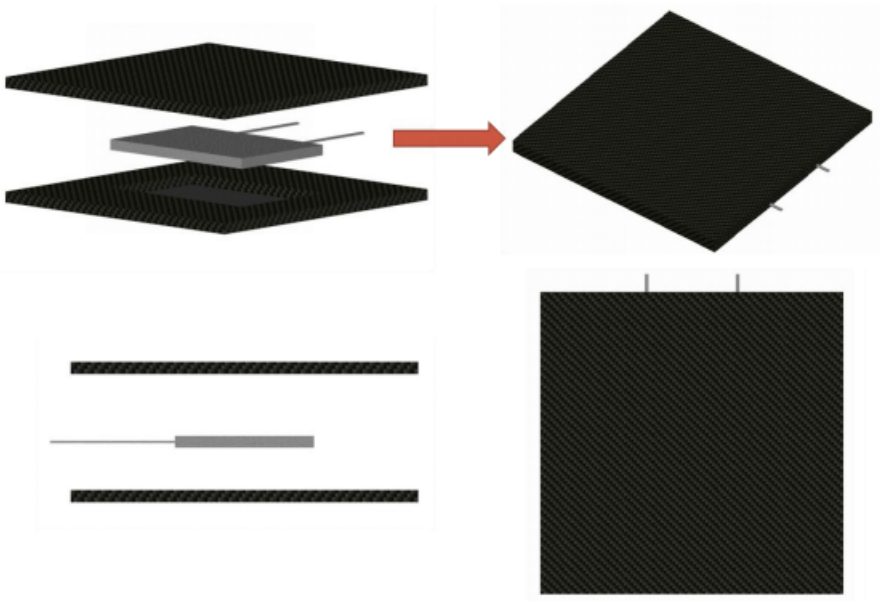

Figure 2.4. Schematic Of CFRP Structure Assembly

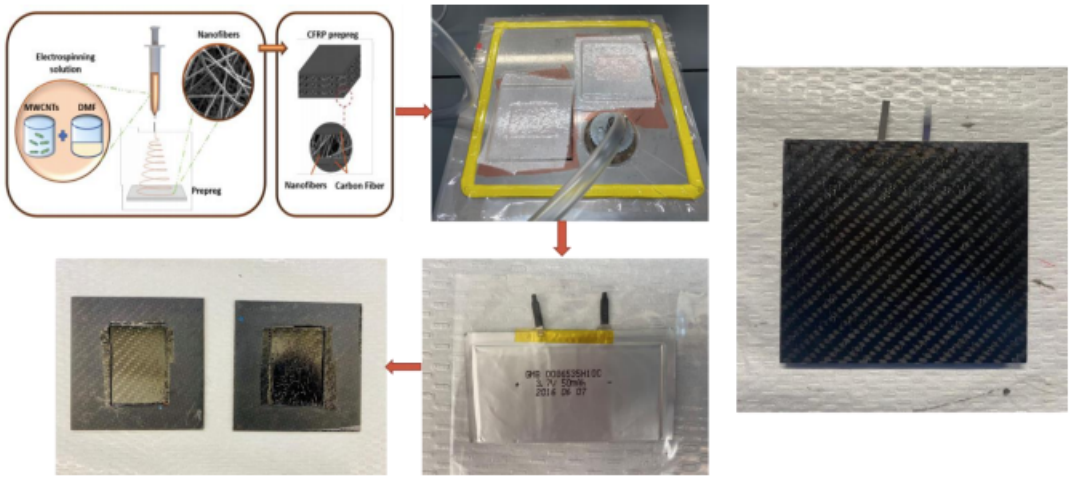

Figure 2.5. Assembly Of CFRP Structure

The second type of sample assembly involves the application of thermoplastic at the center of the two surfaces instead of the uncured prepreg sheet. The thermoplastic sheet was made from Polyethylene-co-acrylic-acid (EAA) ionomer thermoplastic which was compression shaped into a 1.5 mm thick sheet which had a shape of fine pellets to form the barrier layer between the two surfaces. The final sheet was then cut according to the shape of the CFRP face sheet with a square slot in the middle for accommodating the battery. The thermoplastic sheet was then placed on an uncured side of CFRP face sheet and then cured in a programmable oven (Easy Composite, UK) at 120° C. The samples were cured for 25 minutes and vacuuming less than 1 bar. In this manner the thermoplastic sheet becomes homogenized on the CFRP sheet and the adhesion on one side is achieved. The edges of the CFRP facesheets are then heated at a temperature of 70oC by the means of a heat gun. The pouch cell battery is then placed at the center of the surface. Due to the high temperature on the edges of the thermoplastic sheet, it is in melted state acting as the adhesion for the other side of the CFRP face sheet. It becomes easier to join the two surfaces together. The sample is molded in compressed form in a heated hydraulic press to melt further the thermoplastic sheet in the middle layer of the sample and helps to fuse both the surfaces of the facesheets together securely (100oC, 0.5 MPa pressure). Additional epoxy adhesive was applied on the edges to make them smooth and impenetrable on all the sides.

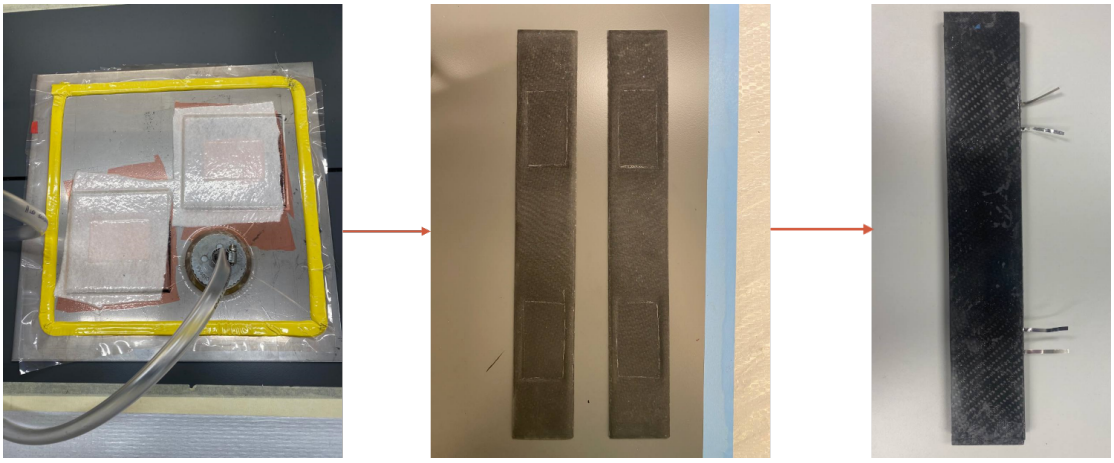

Figure 2.6. Tensile Testing Sample Preparation

2.2 Mechanical Properties

2.2.1 Quasi-Static Three-Point Bending

Three-point bending is performed to define the inter-laminar bond strength characteristics of the various types of CFRP samples. A cylindrical-roller as applicator on the fixture as three-point bending is employed for mechanical testing. (2 kN servo-hydraulic load frame, Integrated Resources Inc. MTS machine). ASTM C393 standard protocol was employed in this testing process. Tensile stress in the convex side and compression stress along the midline are produced in the flexure testing, creating a shear stress area there. Under the three-point loading conditions the force required to bend the beam is measured [5]. The cylindrical load applicator is installed in a manner of the axis parallel to the load applicator axis and axis corresponding to the sample axis. The cylindrical load applicator applied a vertical downward force down the line at mid-span of sample. The evaluation of effective flexural rigidity of the sample is validated through the reinforcement of the inter-layer-shear inhibition capabilities. The load on the sample was applied at 3.33 mm/min. Linear variable differential transducer was employed throughout the experiment to measure the vertical displacement at the mid-span. The initial results of loading were recorded, and the sample was subjected to continuous loading on the mid span for 12 hours. The purpose of this testing is to analyze the battery characteristics for a period of time of continuous bending.

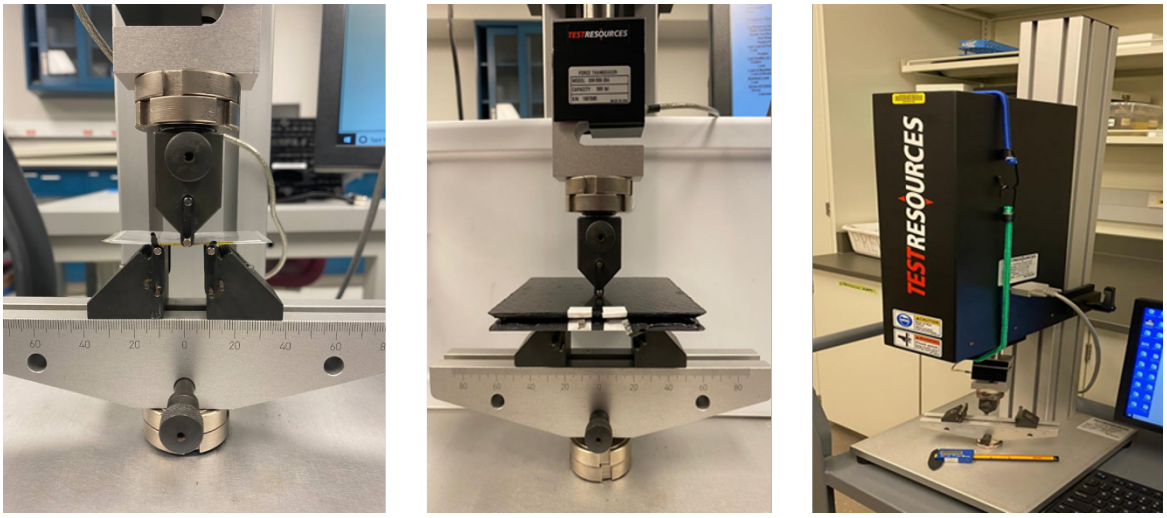

Figure 2.7. Schematic Of Quasistatic Three-Point Bending Testing

2.2.2 Tensile Testing

Tensile testing was performed on the CFRP and Air-Sprayed samples with a provision for two batteries on the ends of both the sides. In this process the ASTM D3039 protocol was employed for testing. It is used to measure the force required to shatter a polymer composite sample to an extent of elongation in order to achieve the breaking point. A stress-strain diagram is the resultant output to determine the tensile modulus. The sample shape was of rectangular stripes with length and width of 35 cm and 5 cm and thickness of 0.6 cm. The sample was placed in the grips of a Universal Test Machine at distance of 5 cm from both the sides and pulled. The loading rate for the sample in this case is 2 mm/min (0.5 in/min) and the testing time observed was 30 seconds. A strain gauge is employed to determine the elongation. Due to the limitation on the highest load available for determining the failure of the samples, load against displacement characteristics were only plotted in the results. As electrospinning of the samples in a rectangular dimension was not feasible, hence air sprayed and conventional CFRP facesheets were only prepared for tensile testing [30].

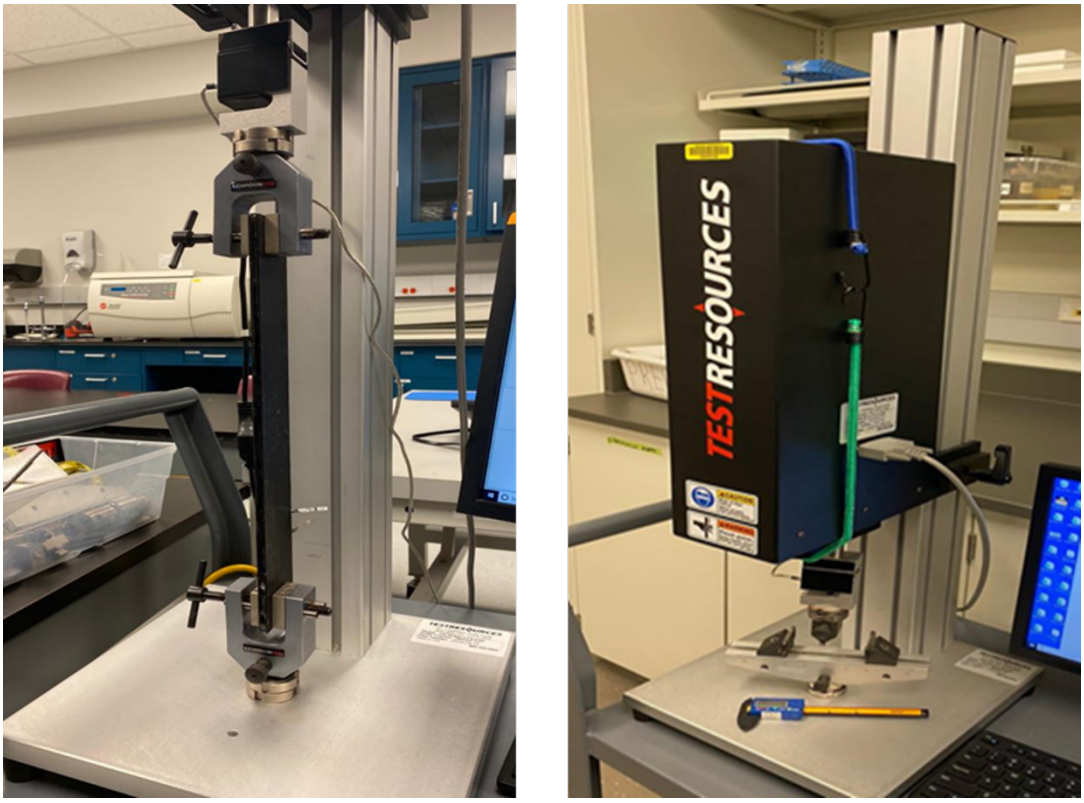

Figure 2.8. Tensile Test Setup

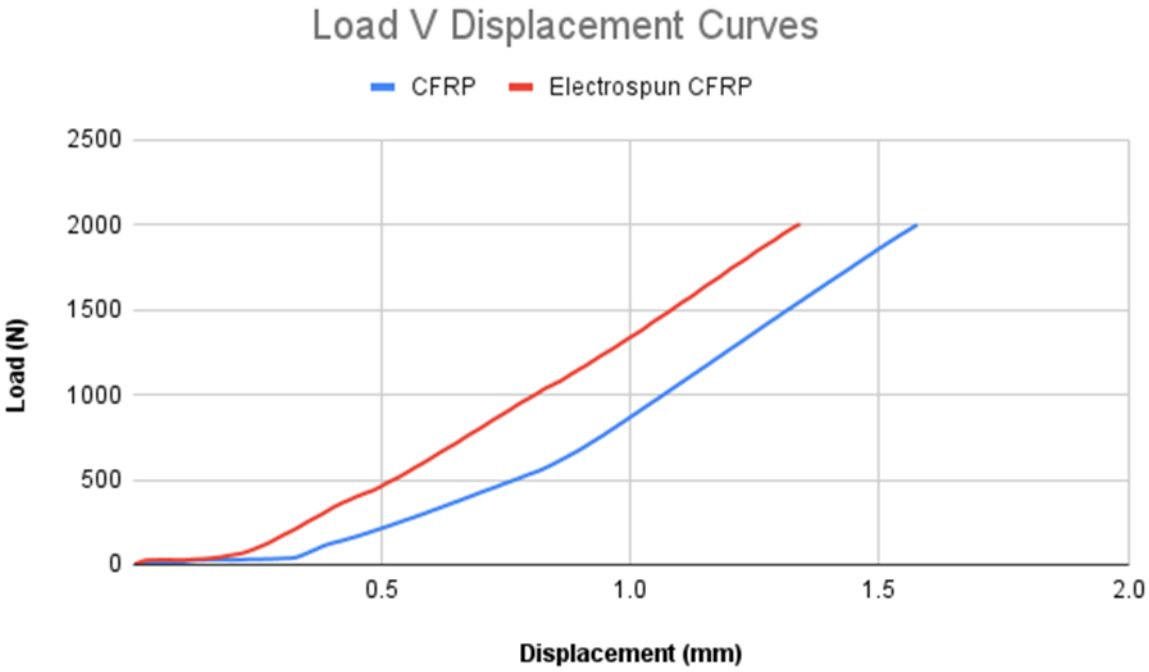

Figure 2.9. Load Vs Displacement Characteristics For Air-Sprayed And CFRP Samples

2.2.3 Barely Visible Impact Damage (BVID)

The samples were placed on a mount and a high-speed DSC-RX10 camera was employed to record impactor displacement, time per revolution. A custom-made aluminum impactor bar having a circular diameter of 10mm is used for conducting the BVID testing. The dimensions of the bar were 72 cm, 1.27 cm and 325 gm in length, width, and weight. The variable nitrogen gas (N2) is utilized to put in force on the impactor. To detect the initial displacement of the impactor a red label was applied on the tip. The recorded images were investigated by an Image-J software. The analysis of the dent was carried out by the energy equation when employed to the baseline CFRP and the impact energy relationship for the dent of electrospun CFRP is compared.

2.2.4 Electrical Conductivity

The Electrospun CFRP, air-sprayed and the conventional samples were gauged for volume electrical resistivity with two probes for Impedance Spectroscopy (Hewlett Packard 4192A LF impedance analyzer, USA). The temperature and relative humidity were set at 220°C and 40% as per the reference from ASTM D257-14. To decrease the surface resistivity a silver paste was applied at the lower and upper surfaces of all the samples which were lightly polished. A copper tape was employed to be a conductor on all the samples to clamp on the system to offer equal contact on the surface. Frequency range from 5 Hz to 13 MHz was computed for sample resistance.

Due to minimal difference between the three samples the resistivity value was arranged at 100 Hz as the resistance. The observed results demonstrated there was no electrical conductivity in the samples because of the presence of epoxy in the layers of the CFRP face sheets. This proves that the LiPo battery packaged within the CFRP structure is safe from any electrical short circuits occurring internally and is not vulnerable to any damage.

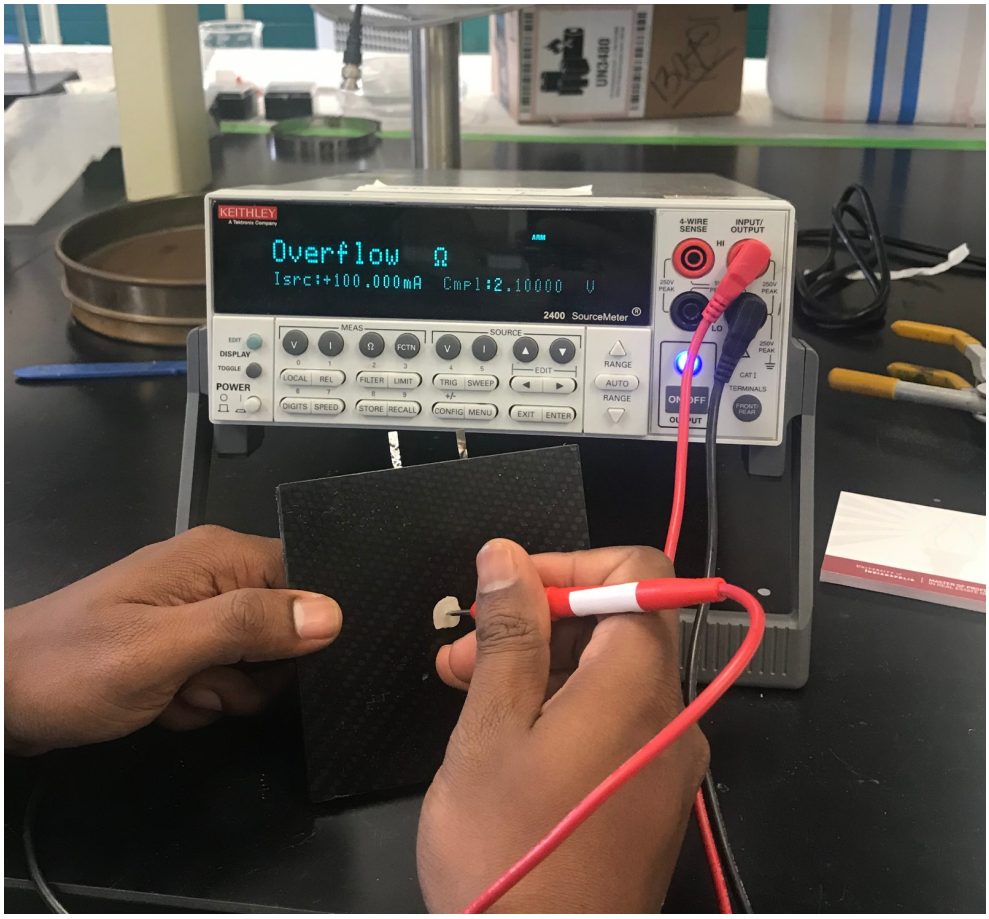

Figure 2.10. Electrical Conductivity Test setup

2.2.5 Electrochemical Characterization

The MESC samples were initially subjected to a continuous maximum bending load for a period of 12 hours. The sample pouch cell battery was also subjected to a bending load until deformation and when it was not under any loading and then tested. The initial purpose was to conduct an in situ testing environment where in the samples were subjected to bending loading and at the same time evaluated for electrochemical performance. But due to the logistical constraints the samples were subjected to the above specific bending cycle and then tested later. The samples were initially exposed to slow rate calibration cycle ranging from 3.0 V and 4.2 V with the intention to define the C rate. The battery is discharged in 1 h at the same current. The preliminary discharge capacity of every sample at the beginning of life (BoL) was measured under continual current (CC) cycling at C/10. The pouch cell

battery is used for this testing so as to record the base performance. This testing is applied to calculate the expected capacity on the quantities of active materials combined. The depth of discharge (DoD) is measured from the voltage discrepancy while the current was interrupted. Then the cells were cycled using a 1C CC profile. This charge-discharge cycle was duplicated to measure the performance of cell life by increasing the cycles of different sample types to compare the discharge capacity retention properties [5].

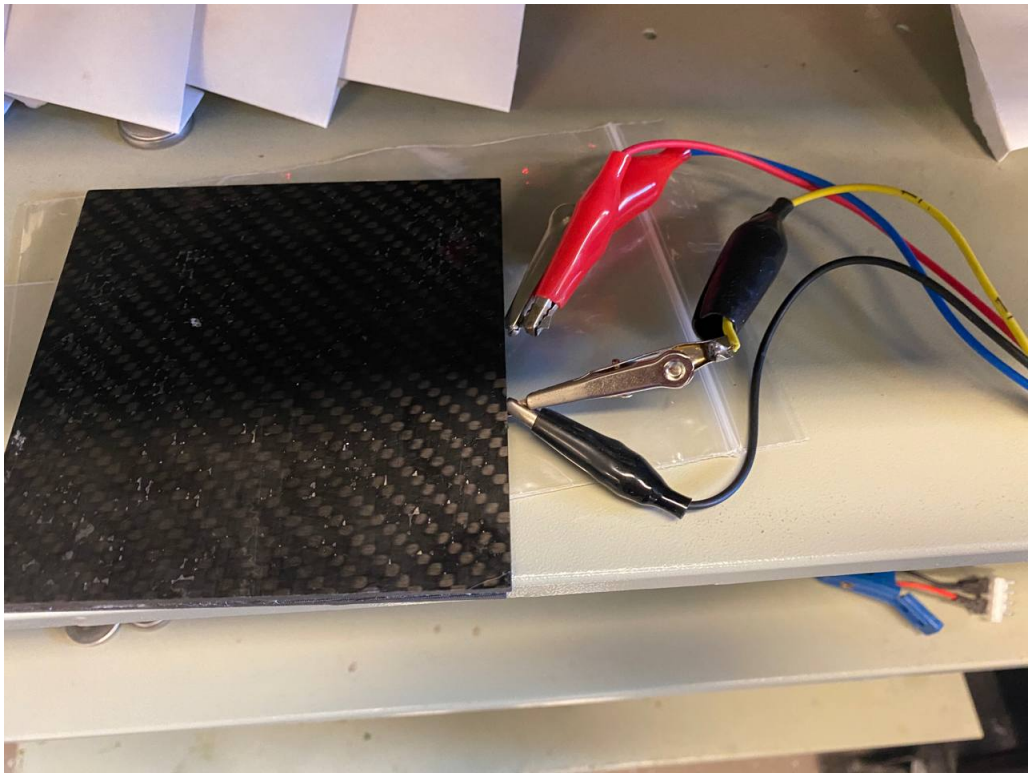

Figure 2.11. MESC Cyclic Testing Setup

3. RESULTS AND DISCUSSION

3.1 Mechanical Properties

3.1.1 Quasi-Static Three-Point Bending Test

The three-point bending for eight cell samples was performed to evaluate the mechanical performance of the MESC within themselves and control pouch cell battery. On the comparison with the other shear tests, the Interlaminar Shear Strength (ILSS) test sampling is much more insistent. The values for flexural stress, elasticity in bending, flexural strain is observed. The results are sensitive to testing method on the basis of specimen, loading geometry and strain rate. In this testing the stress required to fracture the samples yield a slope of stress-deflection curve. The bending moment varies from zero at the support and maximum at the center. The characterization of the six samples was done as follows. Asymmetric and Symmetric orientation. The asymmetric samples were assembled with lesser layers of CFRP on one side than others so the division of 20 layers in all the three samples was twelve layers on the top side and eight layers on the bottom side with the inclusion of adhesion in the middle surface. The electrospun CFRP sample here with 4 wt. % CNT has shown the highest load of 677.82 N in asymmetric orientation and 591.79 N in symmetric orientation samples. The displacement had a limit of 2 mm as it is assumed to be the ideal state where the battery can take the maximum load without affecting its electrochemical characteristics. There is also an observation here that deformation of layers in the top did not occur and this maximum load could be further extended given there was no constraints on the displacement side. On the other hand, the control sample which was fabricated as conventional CFRP sample shows the lowest peak load of 289.38 N with subsequent deformation in its top layers. The air sprayed CFRP sample displays a peak load of 365.25 N and lesser damage in the top layers compared to the conventional CFRP sample. The pouch cell battery could not register a peak load of more than 6 N before being completely deformed.

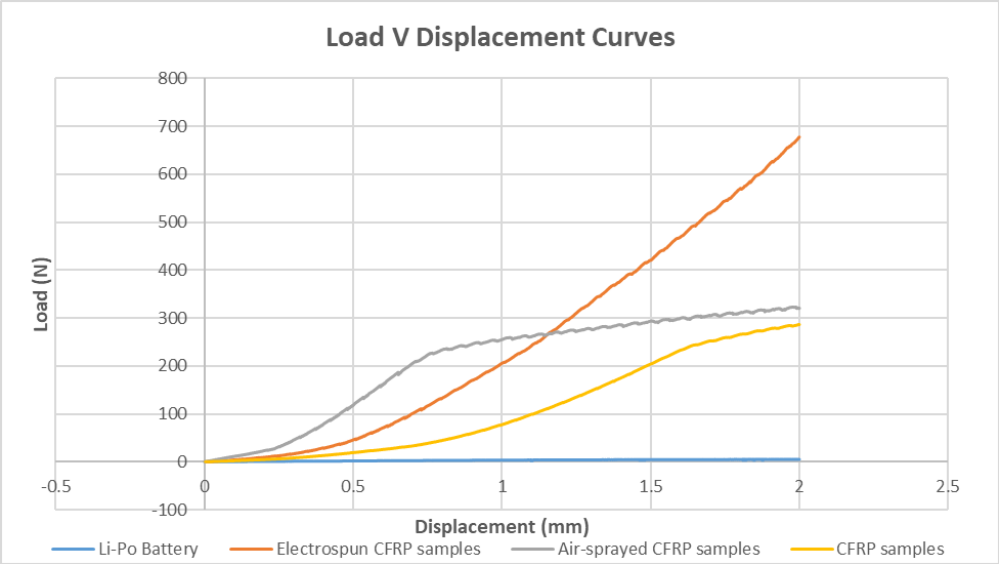

Figure 3.1. Load V Displacement Curves for Asymmetric Orientation Samples

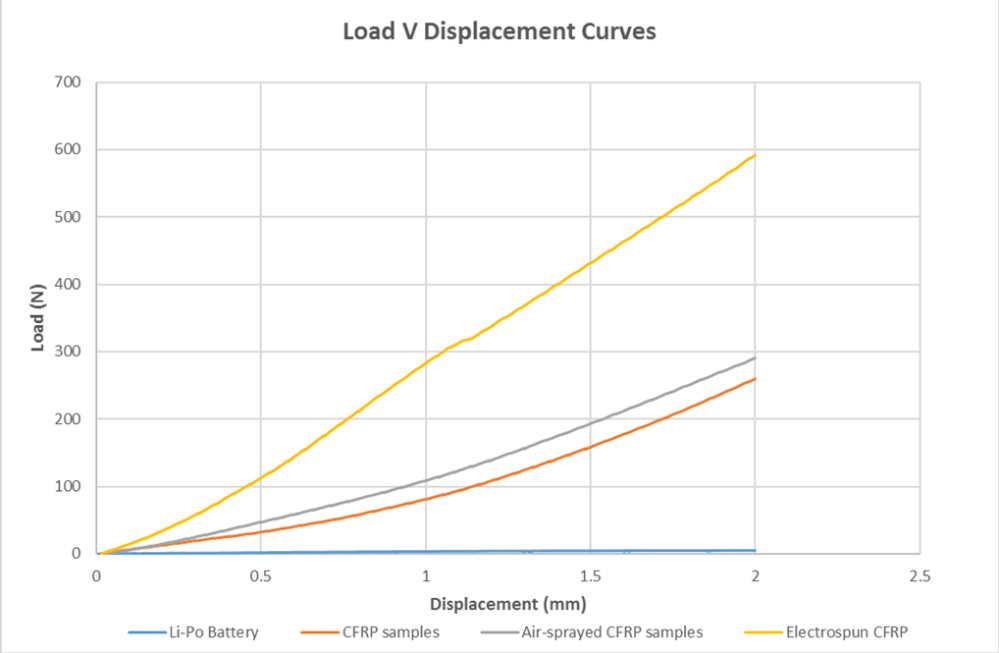

Figure 3.2. Load V Displacement for Symmetric Orientation Samples

The next comparison was between two samples of the same characteristics: Electrospun CFRP sample and the Electrospun CFRP sample with a thermoplastic sheet at its core to act as a packaging method the following are the results of it.

Table 3.1. Comparison between Electrospun and Electrospun Thermoplastic

Sample Type	Electrospun	Electrospun Thermoplastic
Sample Dimensions (L x W) (mm)	(100 x 100)	(100 x 100)
Sample thickness (mm)	5.34	11.58
Sample weight (gm)	63.54	84.35

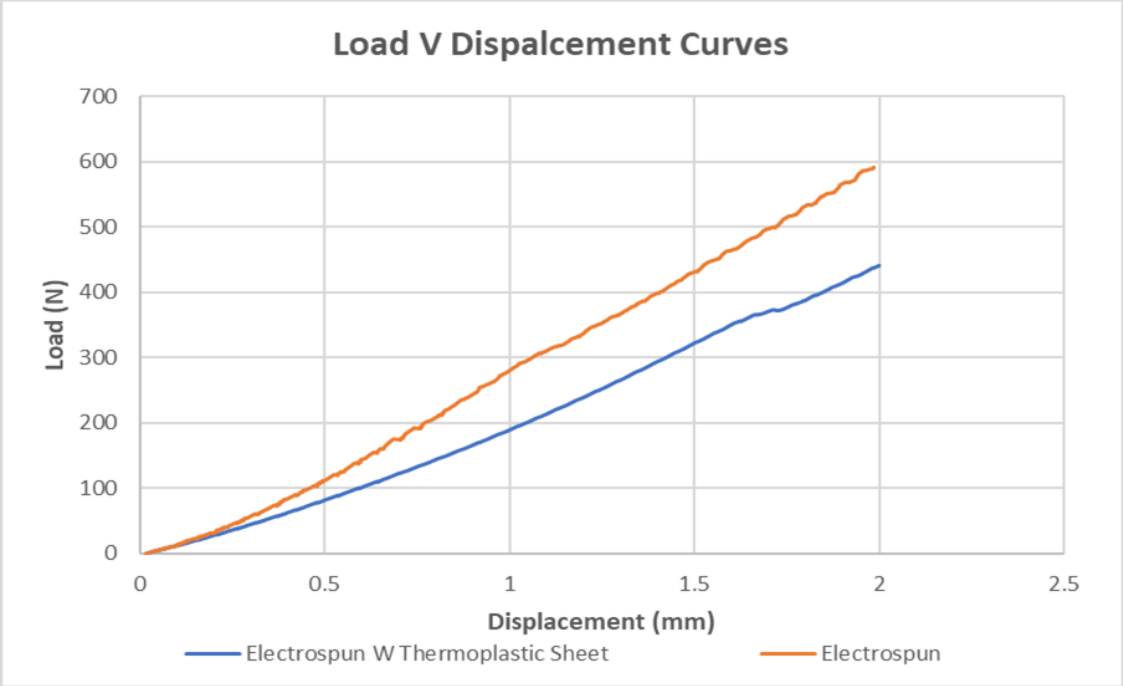

Figure 3.3. Load V Displacement Curves for Comparison between Electrospun CFRP Cell and Electrospun Thermoplastic CFRP Cell

The final comparison involved the peak load carrying capacity between the Electrospun CFRP structure and the conventional CFRP structure without batteries in them and no constraints on the displacement criteria to find out the failure of the two structures. The conventional CFRP structure could withstand a peak load of 1500 N before getting deformed while the Electrospun CFRP structure went up to a peak load of 2000 N.

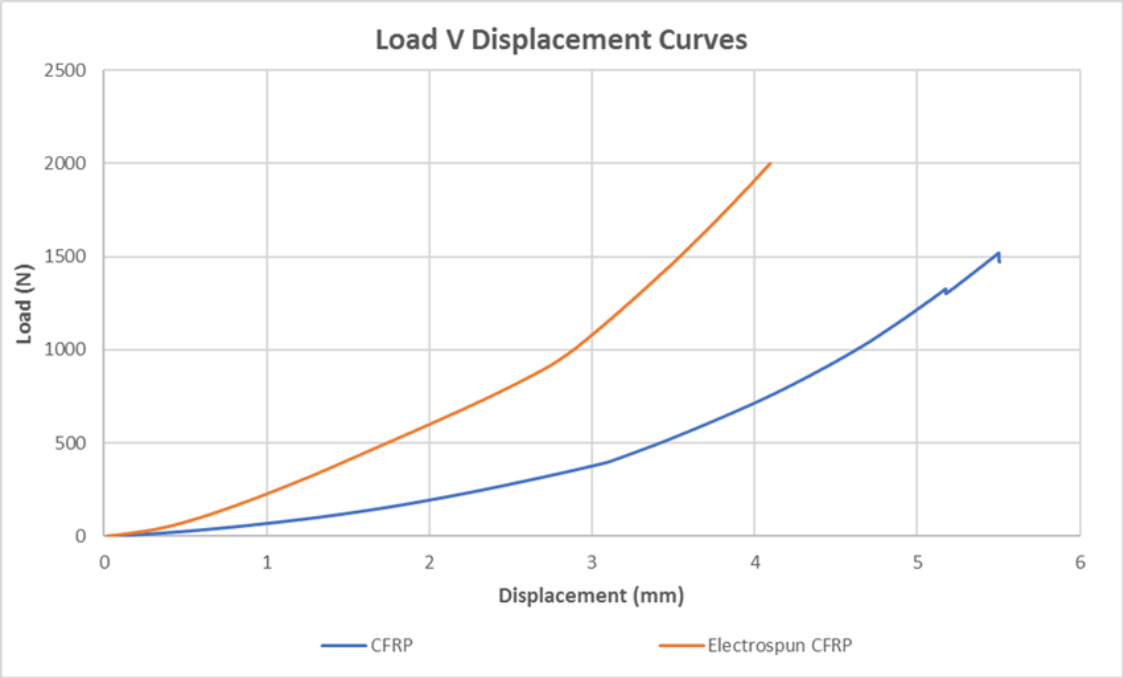

Figure 3.4. Load V Displacement Curves for CFRP Structure Without Batteries

3.1.2 Flexural Rigidity

The most practical method in gauging fiber-resin interface and matrices to assess the improvements in interlaminar properties is the flexural testing. In comparison with the control CFRP and the air sprayed CFRP samples, the electrospun CFRP sample demonstrated elevated flexural strength and strain. The main considerations in this sample were previous research experimentation revealed nano reinforcements integration cause a considerable increase in the flexural properties. The packaging of the lithium-polymer battery in both the symmetric and asymmetric orientation shows a flexural strength of 410.27 psi and goes onto complete deformation while the control and the air-sprayed samples show a flexural strength of 230.15 psi, 390.31 psi and 600.46 psi in the symmetric and asymmetric sample orientations. The highest flexural strength noted for the electrospun sample in the asymmetric and symmetric orientation was 1190.63 psi and 1000.48 psi.

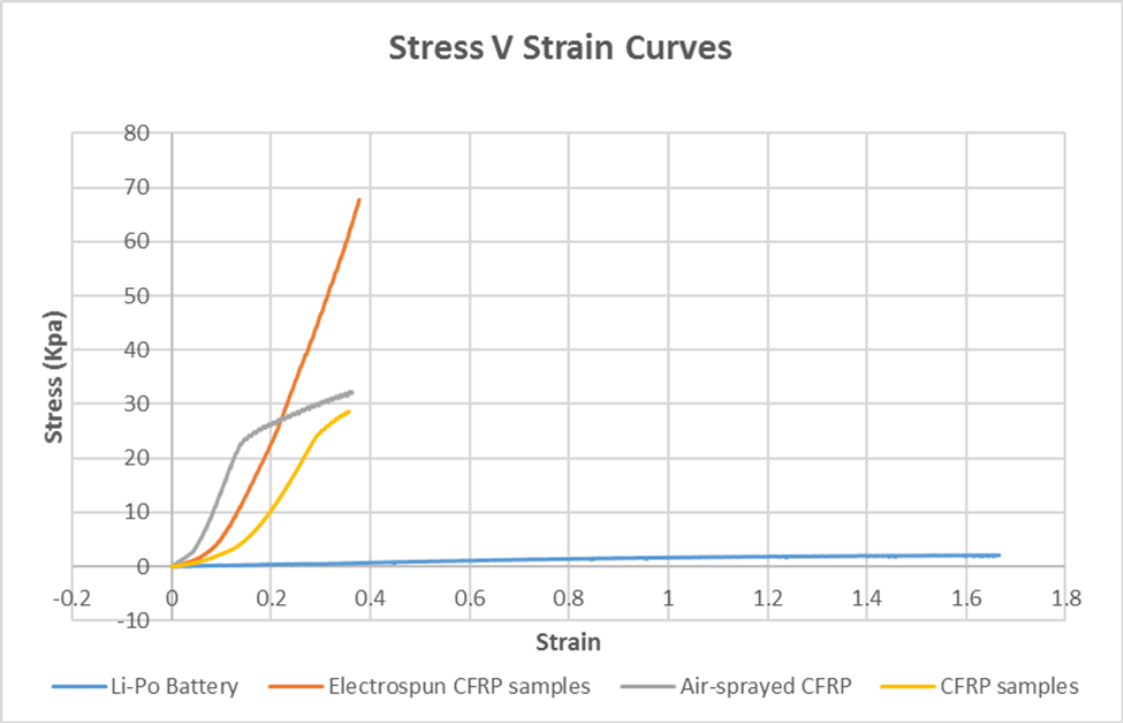

Figure 3.5. Stress V Strain for Asymmetric Orientation Samples

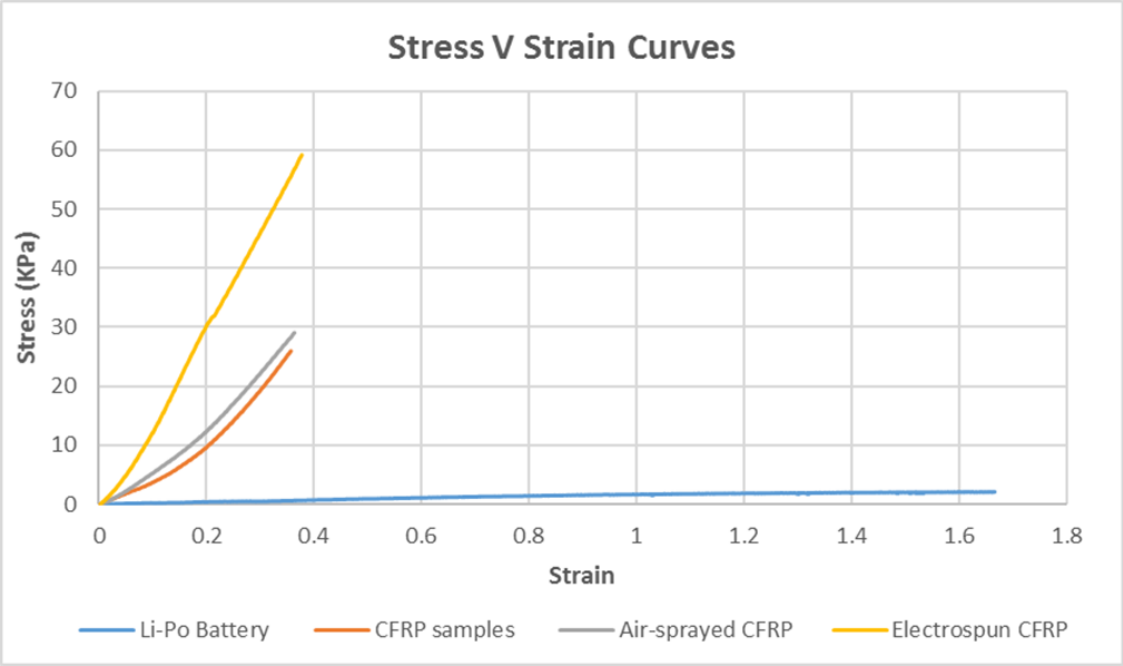

Figure 3.6. Stress V Strain for Symmetric Orientation Samples

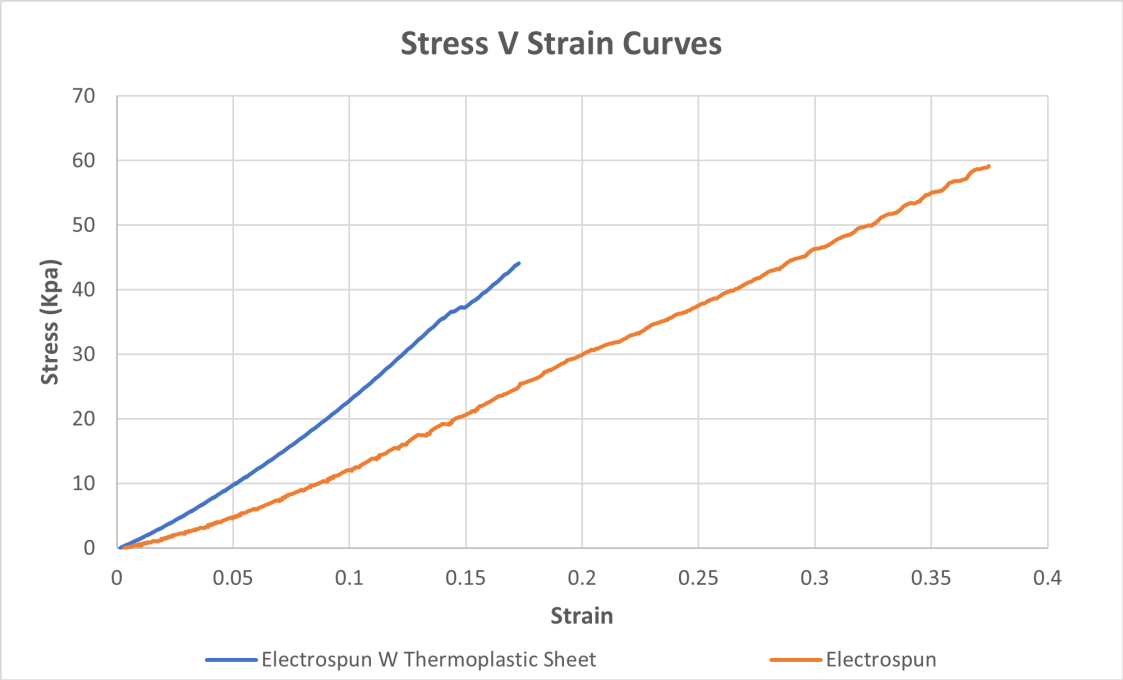

Figure 3.7. Stress V Strain for electrospun and electrospun with thermoplastic sheet insert

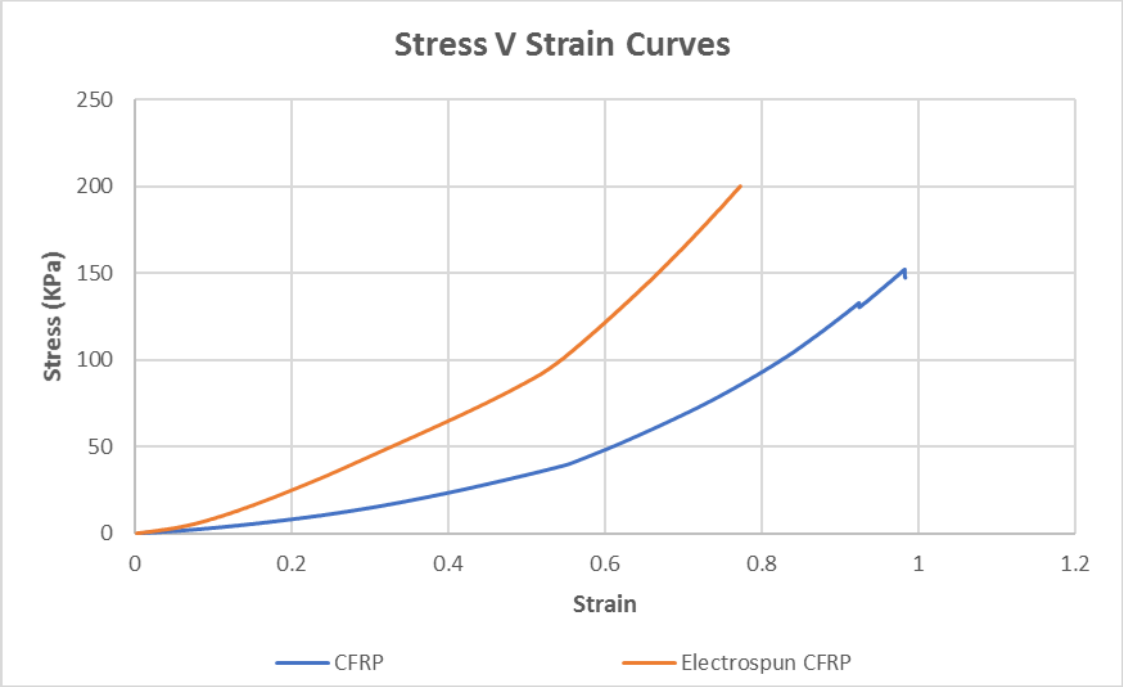

Figure 3.8. Stress V Strain for electrospun and CFRP samples without batteries.

3.1.3 BVID Testing

There are changes in the characteristics of composites like delamination, fiber fracture and matrix cracking over a period of time in usage. Development of such defects is difficult to detect as there is minimal damage on the surface. To have an improved assessment in minimizing these damages in order to prevent catastrophic failures the application of BVID is in place. As per the ASTM standards the Visible Impact Damage (VID) are noticeable at 1.5 mm, but when they are visible at lesser than 1.5 mm they are classified as BVID damages. The observation of the damaged areas implies that a major improvement to the damage resistance is by the engaging EMFs among the composite prepreg layers than the control samples. The electrospun samples show an increase of 7.44 J in impact energy absorption when used with 4 wt.% CNTs ENFs. This proves that when the electrospun samples are compared with the control samples, the delamination resistance is raised by approx. 45% in energy absorption on the composite surface.

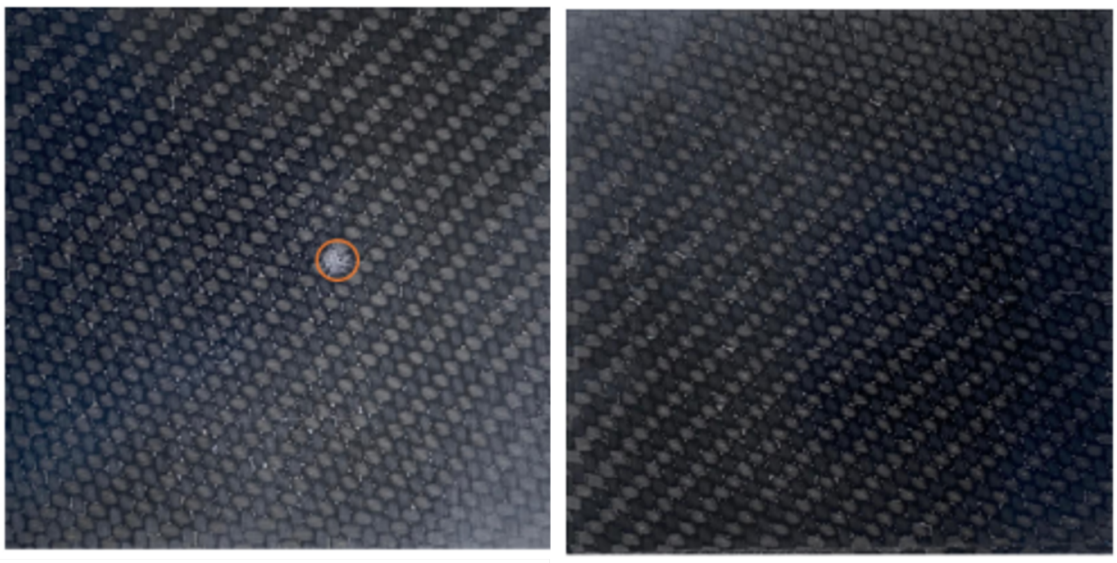

Figure 3.9. CFRP Cell V Electrospun Cell on 16.50 J Impact

3.1.4 Electrochemical Characterization Results

The batteries were cycled in by making use of Landt battery analyzers (Landt Instruments). And all the electrochemical testing was performed at temperature of 30o C. The

pouch cell battery was cycled before and after subjecting to bending loads. The battery failures were not within itself and were caused by the CFRP cells with air-sprayed and the conventional samples, it propagated throughout the entire load-carrying section of the laminate samples and then caused deformation in the batteries. This type of deformation happens from the load applicator in the central region of the structure and still there is no failure of the battery under bending load as the ultimate failure strain of the composites is greater than the pouch cell battery. The voltage (charge or discharge) cycles in conjunction with the battery's capacity values have been taken. It shows that the pouch cell battery and the CFRP cell after the bending show a comparable degradation in the cell capacity after 1C CC. also the voltage profile during charge-discharge cycle is also affected while the pouch cell battery before undergoing bending load and the electrospun CFRP cell show the same electrochemical characteristics in terms of voltage charge/discharge cycling profile and the cell capacity. This proves that overall, the testing characteristics the electrospun CFRP cells are the optimized construction for the MESC.

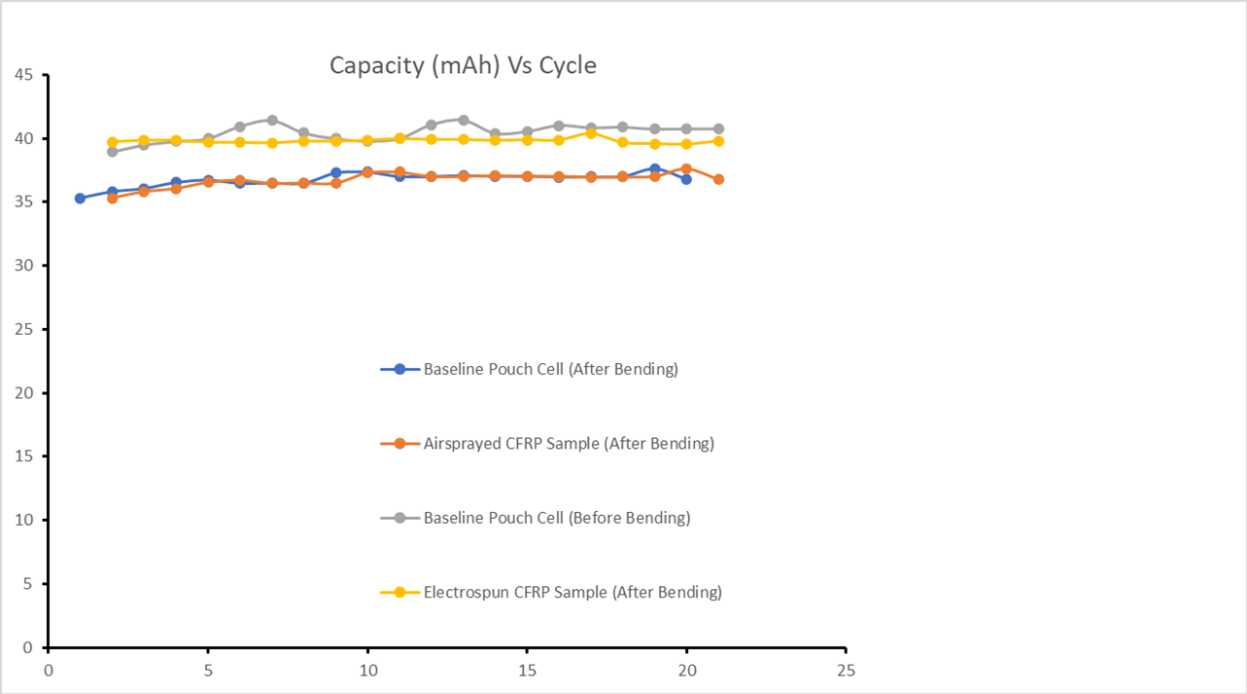

Figure 3.10. Capacity Vs Cycles for MESC Cells

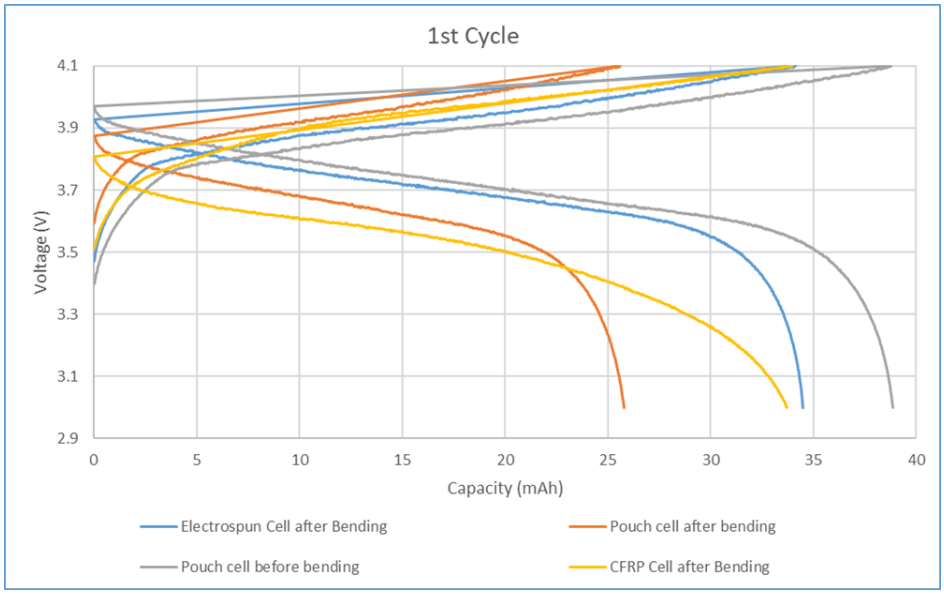

Figure 3.11. Voltage Vs Capacity for 1st Cycle MESC Cells

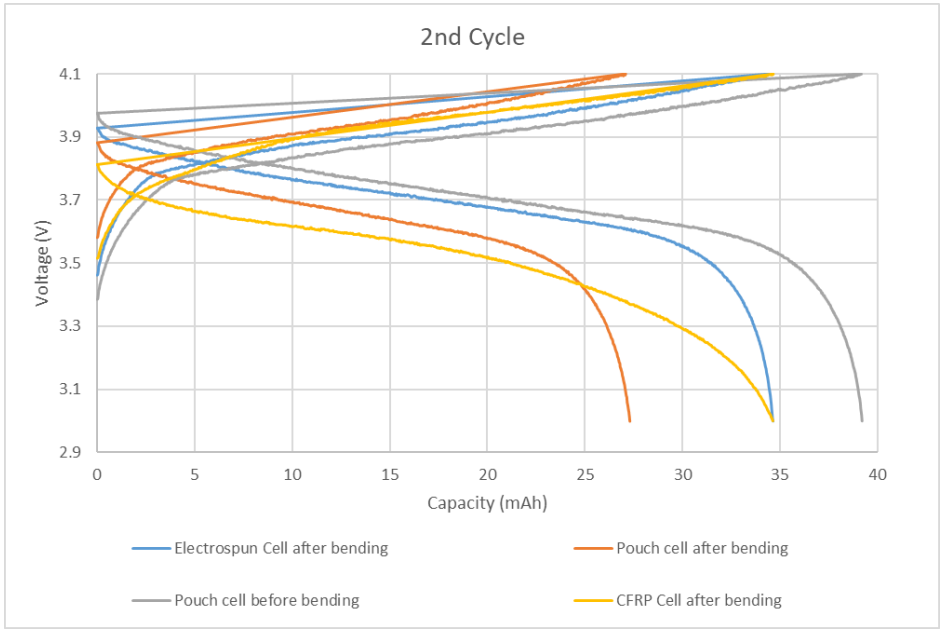

Figure 3.12. Voltage Vs Capacity for 2nd Cycle MESC Cell

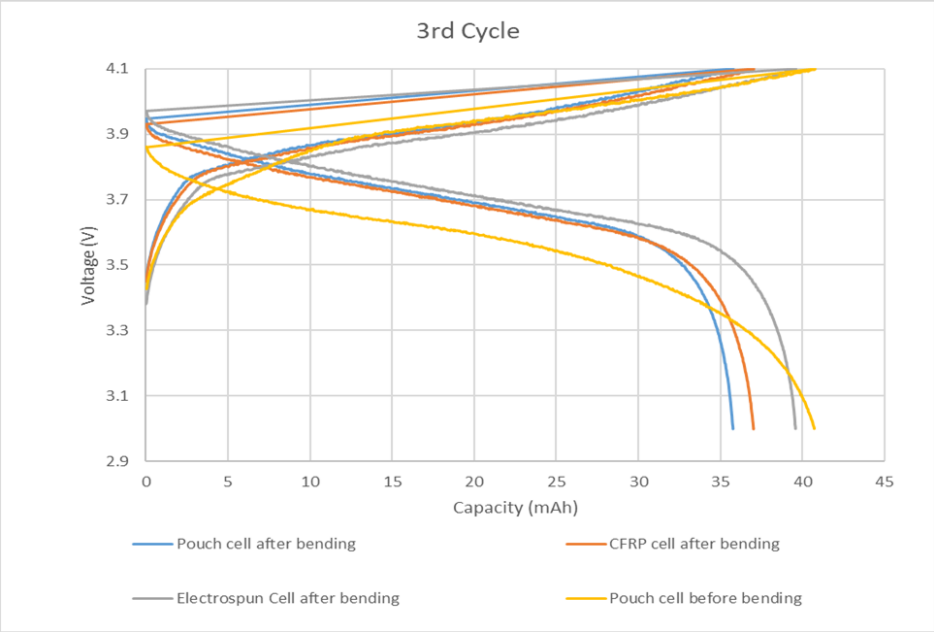

Figure 3.13. Voltage Vs Capacity for 3rd Cycle MESC Cell

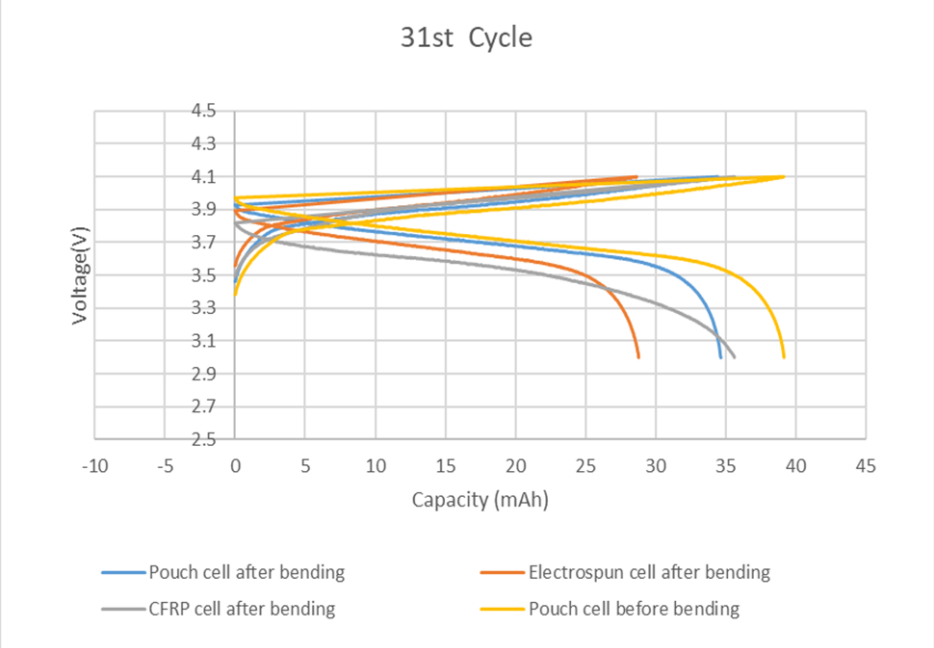

Figure 3.14. Voltage Vs Capacity for 31st Cycle MESC Cell

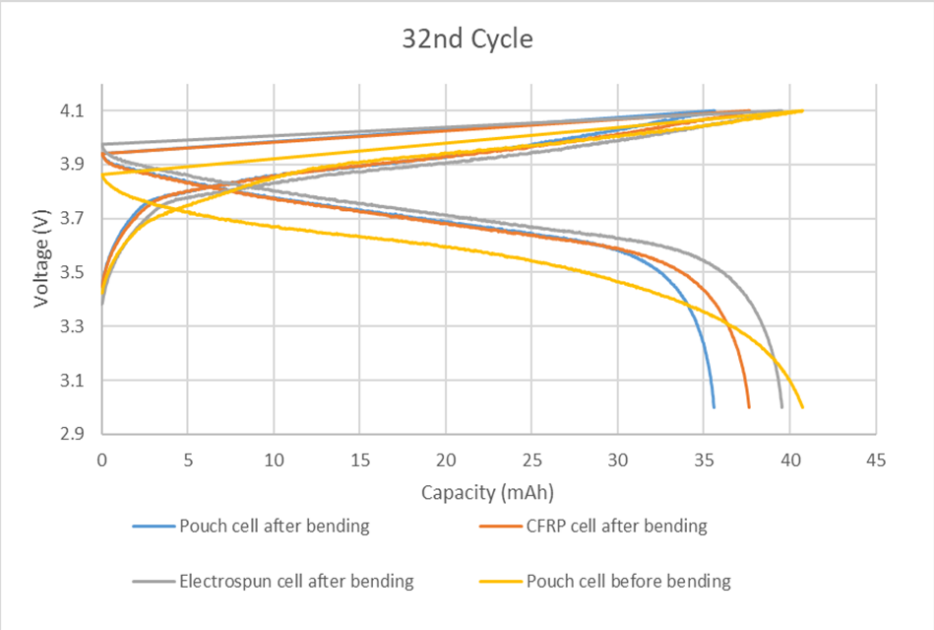

Figure 3.15. Voltage Vs Capacity for 32nd MESC Cell

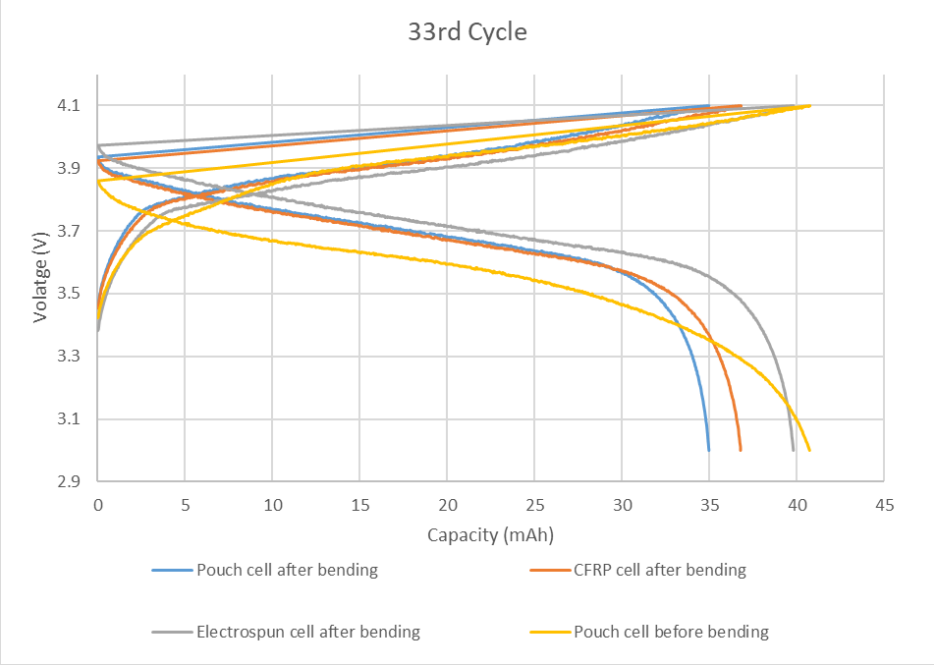

Figure 3.16. Voltage Vs Capacity for 33rd MESC Cell

4. CONCLUSION

The embedding of LiPo batteries inside the sandwich CFRP surfaces core in separate orientation and characteristics present a unique way of structurally embedded batteries in a distinctive material with vertical integration method. In this process fundamental mechanical properties of the CFRP materials makes the industry standard Li-ion battery much more robust in a structural applications environment under the architecture of MESC. All these modifications have no effect on the core battery chemistry and all the battery characteristics remain similar in functionality to that of a pouch cell battery. The inclusion of the batteries in the sandwich composite is not influenced by the bending stiffness in the entire structure. Also, the highest strength in electrospun CFRP.sandwich.structures had no effect on the batteries.when.the possibility of malfunction occurrence was localized metal gouge to the core of the structure. The MESC structure are comprised of three types of CFRP facesheets: the conventional CFRP, air sprayed CFRP and the electrospun CFRP. The unique characteristic of each structure provides better interlayer shear movement and anchors the electrodes of the battery securely to stabilize the loose electrodes which undergo bending loads when there is no packaging present in the external medium. This allows the layers of especially electrospun and the air-sprayed samples to carry on the mechanical loads. The electrochemical characteristics of batteries like the internal resistance, charge/discharge properties and capacity were not distorted during the bending loads and the tensile loading even if the samples were exposed to a possibility of severe failure under deformation by indentation. The results of the mechano-electrical characterization have been presented in this work. There was significant increase in the mass of the sandwich composite with the inclusion of the LiPo batteries since they are much denser and can increase the self-weight of the structure and also can decrease the strength and stiffness at the same time. The design consideration in this case can be an equilibrium of particular properties and aim on increasing the energy storage density for obtaining the lightweight structures. This was proven correct by the electrospun CFRP samples which were comparatively lighter in weight than the air-sprayed and conventional samples and thinner in construction resulting in maximum mechanical strength.

5. OPPORTUNITIES AND FUTURE RESEARCH

The energy storage sector has noticed a significant evolution from developing electricity in a central supply to systems completely favored by compact batteries. The reason for this development is the commercial growth of lithium-ion battery electricity and the various storage media associated with it. This will likely see amendments in the visibly situated systems like integrated structural, flexible, wearable, and multifunctional materials. Likewise, the improvement in form factor of energy storage devices can facilitate a modern technological advancement in power incorporated systems and materials. It poses a fundamental challenge on the functionality of battery systems. The air exposure is major factor in the operation of electrodes and electrolytes and its absence determines the sensitivity of the batteries.

The scientific research and publications in the field of electrospinning of carbon fiber filaments for improving the existing properties of the composite materials demonstrates that it is at a rapid level, and it impacts the properties like alignment, aspect ratio, fiber diameters, interfacial interactions. Its addition in the conventional composites has enhanced the impact resistance, flexural strength and impact damping characteristics. There are challenges in manufacturing processes for obtaining the interfacial interactions of the fibers and their layup and alignment properties. As there is less production of these structurally advanced composites, the major obstacle is to make the leap from lab environment to the commercial industries. The production cost is another area where feasibility of the application matters and can be researched further for impactful results [37].

The current work can be developed further into designing multifunctional materials which can be treated as composite materials although at the same time act as structural and energy storage with dual properties. Hence researchers have taken the initiative to package lithium battery materials into structural templates. The approaches towards working in this specific direction includes construction of electrodes from carbon fiber but it becomes bulky upon addition of reinforcements for improving mechanical properties. Another approach can be made towards application of carbon fiber materials as the lithium battery anodes and design a packaging method to sustain the modular elements while keeping the feasibility of the final product as per its application in the commercial space.

REFERENCES

[1] R. F. Gibson, "A review of recent research on mechanics of multifunctional composite materials and structures," *Composite structures*, vol. 92, no. 12, pp. 2793–2810, 2010.

[2] J. P. Thomas and M. A. Qidwai, "Mechanical design and performance of composite multifunctional materials," *Acta materialia*, vol. 52, no. 8, pp. 2155–2164, 2004.

[3] E. D. Wetzel, "Reducing weight: Multifunctional composites integrate power, communications and structure," *AMPTIAC Q*, vol. 8, no. 4, pp. 91–95, 2004.

[4] L. E. Asp, S. Leijonmarck, T. Carlson, and G. Lindbergh, "Realisation of structural battery composite materials," in *20th International Conference on Composite Materials (Proceedings)*, 2015, pp. 1121–1122.

[5] P. Ladpli, R. Nardari, F. Kopsaftopoulos, and F.-K. Chang, "Multifunctional energy storage composite structures with embedded lithium-ion batteries," *Journal of Power Sources*, vol. 414, pp. 517–529, 2019.

[6] J. Neubauer, A. Pesaran, C. Bae, R. Elder, and B. Cunningham, "Updating united states advanced battery consortium and department of energy battery technology targets for battery electric vehicles," *Journal of Power Sources*, vol. 271, pp. 614–621, 2014.

[7] T. Reinhart, "Overview of composite materials," in *Handbook of composites*, Springer, 1998, pp. 21–33.

[8] G. Di Bella, V. Fiore, and A. Valenza, "Natural fiber-reinforced composites," 2012.

[9] R. M. Guedes and J. Xavier, "Understanding and predicting stiffness in advanced fibre-reinforced polymer (frp) composites for structural applications," in *Advanced Fibre-Reinforced Polymer (FRP) Composites for Structural Applications*, Elsevier, 2013, pp. 298–360.

[10] S. U. Khan and J.-K. Kim, "Impact and delamination failure of multiscale carbon nanotube-fiber reinforced polymer composites: A review," *International Journal of Aeronautical and Space Sciences*, vol. 12, no. 2, pp. 115–133, 2011.

[11] T. Yokozeki, Y. Iwahori, S. Ishiwata, and K. Enomoto, "Mechanical properties of cfrp laminates manufactured from unidirectional prepregs using cscnt-dispersed epoxy," *Composites Part A: Applied Science and Manufacturing*, vol. 38, no. 10, pp. 2121–2130, 2007.

[12] M. Mirjalili and S. Zohoori, "Review for application of electrospinning and electrospun nanofibers technology in textile industry," *Journal of Nanostructure in Chemistry*, vol. 6, no. 3, pp. 207–213, 2016.

[13] H. Esfahani, R. Jose, and S. Ramakrishna, "Electrospun ceramic nanofiber mats today: Synthesis, properties, and applications," *Materials*, vol. 10, no. 11, p. 1238, 2017.

[14] T. Christen and M. W. Carlen, "Theory of ragone plots," *Journal of power sources*, vol. 91, no. 2, pp. 210–216, 2000.

[15] P. J. Hall and E. J. Bain, "Energy-storage technologies and electricity generation," *Energy policy*, vol. 36, no. 12, pp. 4352–4355, 2008.

[16] S. Koohi-Fayegh and M. A. Rosen, "A review of energy storage types, applications and recent developments," *Journal of Energy Storage*, vol. 27, p. 101 047, 2020.

[17] H. Chen, T. N. Cong, W. Yang, C. Tan, Y. Li, and Y. Ding, "Progress in electrical energy storage system: A critical review," *Progress in natural science*, vol. 19, no. 3, pp. 291–312, 2009.

[18] E. Sahraei, R. Hill, and T. Wierzbicki, "Calibration and finite element simulation of pouch lithium-ion batteries for mechanical integrity," *Journal of Power Sources*, vol. 201, pp. 307–321, 2012.

[19] H. Luo, Y. Xia, and Q. Zhou, "Mechanical damage in a lithium-ion pouch cell under indentation loads," *Journal of Power Sources*, vol. 357, pp. 61–70, 2017.

[20] E. Sahraei, J. Campbell, and T. Wierzbicki, "Modeling and short circuit detection of 18650 li-ion cells under mechanical abuse conditions," *Journal of Power Sources*, vol. 220, pp. 360–372, 2012.

[21] E. Sahraei, J. Meier, and T. Wierzbicki, "Characterizing and modeling mechanical properties and onset of short circuit for three types of lithium-ion pouch cells," *Journal of Power Sources*, vol. 247, pp. 503–516, 2014.

[22] E. Sahraei, M. Kahn, J. Meier, and T. Wierzbicki, "Modelling of cracks developed in lithium-ion cells under mechanical loading," *Rsc Advances*, vol. 5, no. 98, pp. 80 369–80 380, 2015.

[23] Y. Zhao, D. Zhao, T. Zhang, H. Li, B. Zhang, and Z. Zhenchong, "Preparation and multifunctional performance of carbon fiber-reinforced plastic composites for laminated structural batteries," *Polymer Composites*, vol. 41, no. 8, pp. 3023–3033, 2020.

[24] W. Johannisson, N. Ihrner, D. Zenkert, M. Johansson, D. Carlstedt, L. E. Asp, and F. Sieland, "Multifunctional performance of a carbon fiber ud lamina electrode for structural batteries," *Composites Science and Technology*, vol. 168, pp. 81–87, 2018.

[25] S. Shalouf, J. Zhang, and C. Wang, "Effects of mechanical deformation on electric performance of rechargeable batteries embedded in load carrying composite structures," *Plastics, Rubber and Composites*, vol. 43, no. 3, pp. 98–104, 2014.

[26] J. Thomas, S. Qidwai, W. Pogue III, and G. Pham, "Multifunctional structure-battery composites for marine systems," *Journal of Composite Materials*, vol. 47, no. 1, pp. 5–26, 2013.

[27] P. Attar, J. Galos, A. Best, and A. Mouritz, "Compression properties of multifunctional composite structures with embedded lithium-ion polymer batteries," *Composite Structures*, vol. 237, p. 111 937, 2020.

[28] A. D. B. Ferreira, P. R. Nóvoa, and A. T. Marques, "Multifunctional material systems: A state-of-the-art review," *Composite Structures*, vol. 151, pp. 3–35, 2016.

[29] F. Gasco and P. Feraboli, "Manufacturability of composite laminates with integrated thin film li-ion batteries," *Journal of composite materials*, vol. 48, no. 8, pp. 899–910, 2014.

[30] K. Pattarakunnan, J. Galos, R. Das, and A. Mouritz, "Tensile properties of multifunctional composites embedded with lithium-ion polymer batteries," *Composites Part A: Applied Science and Manufacturing*, vol. 136, p. 105 966, 2020.

[31] D. ASTM, "7137/d 7137m-05. standard test method for compressive residual strength properties of damaged polymer matrix composite plates," *Annual book of ASTM standards*, 2005.

[32] E. Jones, "Documentation for matlab-based dic code," *University or Illinois*, 2013.

[33] J. Galos, A. A. Khatibi, and A. P. Mouritz, "Vibration and acoustic properties of composites with embedded lithium-ion polymer batteries," *Composite Structures*, vol. 220, pp. 677–686, 2019.

[34] N. Aliahmad, P. K. Biswas, V. Wable, I. Hernandez, A. Siegel, H. Dalir, and M. Agarwal, "Electrospun thermosetting carbon nanotube–epoxy nanofibers," *ACS Applied Polymer Materials*, vol. 3, no. 2, pp. 610–619, 2020.

[35] V. Wable, P. K. Biswas, R. Moheimani, N. Aliahmad, P. Omole, A. P. Siegel, M. Agarwal, and H. Dalir, "Engineering the electrospinning of mwcnts/epoxy nanofiber scaffolds to enhance physical and mechanical properties of cfrps," *Composites Science and Technology*, p. 108 941, 2021.

[36] P. K. Biswas, N. Aliahmad, H. Dalir, and M. Agarwal, "Nanostructured v2o5-swcnts based lithium ion battery for multifunctional energy storage composites: Materials synthesis and fabrication," in *AIAA Scitech 2021 Forum*, 2021, p. 1006.

[37] K. Moyer, C. Meng, B. Marshall, O. Assal, J. Eaves, D. Perez, R. Karkkainen, L. Roberson, and C. Pint, "Carbon fiber reinforced structural lithium-ion battery composite: Multifunctional power integration for cubesats," English (US), *Energy Storage Materials*, vol. 24, pp. 676–681, Jan. 2020, ISSN: 2405-8297. DOI: 10.1016/j.ensm.2019.08.003.